An evolutionary compass for elucidating selection mechanisms shaping complex traits

Lawrence H. Uricchio,[1*†] Hugo C. Kitano,[2*]
Alexander Gusev,[3‡] Noah A. Zaitlen[4,5‡†∓]

Departments of [1]Biology and [2]Computer Science, Stanford University, Stanford, CA; [3]Dana Farber Cancer Institute, Boston, MA; Departments of [4]Medicine and [5]Bioengineering and Therapeutic Sciences, University of California, San Francisco, CA

[*]These authors contributed equally to this work
[‡]These authors contributed equally to this work
[†]To whom correspondence should be addressed: uricchio@stanford.edu, noah.zaitlen@ucsf.edu
[∓]Lead contact: noah.zaitlen@ucsf.edu

Polygenic selection is likely to target some human traits, but the specific evolutionary mechanisms driving complex trait variation are largely unknown. We developed an evolutionary compass for detecting selection and mutational bias that uses polarized GWAS summary statistics from a single population. We found evidence for selection and mutational bias acting on variation in five traits (BMI, schizophrenia, Crohn's disease, educational attainment, and height). We then used model-based analyses to show that these signals can be explained by stabilizing selection with shifts in the fitness-phenotype relationship. We additionally provide evidence that selection has acted on Neanderthal alleles for height, schizophrenia, and depression, and discuss potential sources of confounding. Our results provide a flexible and powerful framework for evolutionary analysis of complex phenotypes in humans and other organisms, and provide insights into the evolutionary mechanisms driving variation in human polygenic traits.

Introduction

Natural selection shapes variation within and between human populations, but the phenotypic targets of selection and the evolutionary mechanisms shaping causal variation for selected traits remain largely unknown. Most studies of selection in humans have focused on classic selective sweeps (Sabeti et al., 2002; Voight et al., 2006; Sabeti et al., 2006; Hernandez et al., 2011; Enard et al., 2014), but other processes such as stabilizing selection (Gilad et al., 2006; Sanjak et al., 2017b), polygenic adaptation (Turchin et al.,

2012; Berg and Coop, 2014), and soft sweeps (Messer and Petrov, 2013) may also play an important role in shaping human diversity. Methods to detect selection under these more complex models are needed if we are to fulfill the promise of genomics to explain the evolutionary mechanisms driving the distribution of heritable traits in human populations (Pritchard et al., 2010).

With the recent proliferation of paired genotype and phenotype data from large human cohorts, it is now feasible to test for polygenic selection on specific traits (Turchin et al., 2012; Berg and Coop, 2014; Yang et al., 2015; Robinson et al., 2015; Field et al., 2016). While these studies have provided strong evidence that polygenic selection is likely to be an important determinant of variation in traits such as height and skin pigmentation (Berg and Coop, 2014), important questions remain about the evolutionary mechanisms that drive complex trait variation. In particular, most previous studies of selection on human complex traits have focused either on polygenic adaptation (Turchin et al., 2012; Berg and Coop, 2014; Field et al., 2016; Berg et al., 2017; Racimo et al., 2018) or stabilizing/negative selection (Yang et al., 2015; Zeng et al., 2018; Simons et al., 2018), and have not incorporated mutational bias (*i.e.*, the propensity for new mutations to be preferentially trait-increasing or preferentially trait-decreasing). To detect polygenic adaptation, studies have relied on genotype data from multiple populations to probe the frequency and linkage properties of trait-associated alleles as compared to a null based on genome-wide SNPs (Turchin et al., 2012; Berg and Coop, 2014; Racimo et al., 2018), or have used haplotype-based statistics and dense sequence data from a single population (Field et al., 2016). Negative selection has been investigated by comparing empirical data to null models of the relationship between frequency and squared effect sizes (Schoech et al., 2017) or linkage disequilibrium and per-SNP heritability (Gazal et al., 2017). These studies have argued that selection acts on many traits, and that both negative (Gazal et al., 2017; Schoech et al., 2017) and positive (Berg and Coop, 2014; Berg et al., 2017) selection act on complex traits such as height and BMI.

While each of these approaches has provided insights into the evolution of complex traits, a more comprehensive view of trait evolution will require methods that can account for pleiotropic selection and incorporate signals of both adaptive and deleterious selection processes simultaneously. Recent progress has been reported in accounting for higher dimensional trait spaces (Berg et al., 2017; Simons et al., 2018), but there is a need for models and inference tools integrating signatures of positive and negative selection on complex traits (Sanjak et al., 2017b). Indeed, a natural way to model polygenic adaptation is to view stabilizing selection as a null process, with punctuated changes in the fittest trait value (herein called the "optimal trait value" or "trait optimum") driving brief periods of adaptation (Barton, 1986; Jain and Stephan, 2017). Mutational bias may also be an important contributor to the evolutionary dynamics of complex traits (Charlesworth, 2013), but has not been directly incorporated into recent

empirical studies. If there is a bias in the direction of effect of *de novo* mutations, populations may carry less standing variation for alleles that alter the phenotype in one direction than the other, potentially altering the dynamics of future adaptation to changes in the trait optimum. Moreover, biases in mutation rate for selected traits may induce detectable patterns in the relationship between allele frequency and effect size.

Here, we develop a powerful method for detecting mutational bias and selection within a single population using GWAS summary data. We show that the polarization of GWAS summary statistics by their ancestral/derived state or Neanderthal/modern human state (which we refer to as an "evolutionary compass") provides information about the evolutionary processes shaping trait variation. We propose a simple summary statistic of the relationship between effect sizes and allele frequency, and show that it is sensitive to both mutational bias and various models of selection. We apply our approach and find that selection and mutational bias are likely to have acted on the genetic variation underlying height, BMI, educational attainment, Crohn's disease, and schizophrenia, as well as Neanderthal alleles for height, depression, and schizophrenia. We then develop a model-based inference procedure to disentangle mutational bias from selection, and show that both processes are necessary to explain the observed GWAS summary data. Lastly, we discuss caveats and possible explanations for idiosyncratic patterns in height summary statistics across independent cohorts, as well as implications of our findings for human evolutionary history and GWAS of biomedically relevant traits.

Results

An evolutionary compass for GWAS. Associations between genotypes and complex traits are usually reported with respect to a reference allele that is arbitrarily chosen, which can obscure the direction of effect of new mutations. When selection acts on traits, it favors the reproductive success or survival of individuals with particular trait values, implying that the fitness effect of new mutations may depend on both the sign and magnitude of their impact on a selected trait. Therefore, we choose ancestral alleles as the reference state and explore the relationship between derived allele effect sizes and derived allele frequency, which we encode in a βDAF plot (*i.e.*, a plot encoding the relationship between the mean value of effect sizes β estimated in a GWAS ($\bar{\beta}$) and derived allele frequency (DAF); Fig. 1). Note that we use estimated effect sizes from all alleles to compute $\bar{\beta}$, regardless of their significance.

A βDAF plot contains information about mutational bias and selection on the trait of interest. While many forms of selection will induce patterns in the βDAF plot (including mutational bias alone and directional selection, which we explore in the Supplemental Information with simulations and analytical

calculations), we consider an example of stabilizing selection with shifts in the optimal trait value for illustrative purposes. Stabilizing selection is typically parameterized by several parameters, but here we focus on the optimal phenotype value, ϕ_o, which represents the value of the phenotype that confers the highest fitness. Applying a classic stabilizing selection model, we suppose that fitness is controlled by a Gaussian function centered at ϕ_o (Robertson, 1956; Barton, 1986; Simons et al., 2018) (Fig 1A). In addition, we suppose that trait-increasing mutations may be more or less likely than trait-decreasing mutations, which we capture with the parameter δ (defined as the proportion of trait-altering *de novo* mutations that increase trait values), and that ϕ_o can change, inducing a brief period of adaptation in which trait values equilibrate to a new optimal value.

We performed forward simulations of complex traits under this model and explored how various evolutionary parameters affect the properties of a βDAF plot. Although we consider a very large range of possible parameter combinations when performing statistical inference in later sections, here we focused on 4 models, including one model of stabilizing selection in the absence of shifts in the optimal trait value, and three models that varied the timing of a shift in the optimal trait value ϕ_o (Fig. 1C). All of the models included a bias in mutation rate towards trait-decreasing alleles ($\delta = 0.4$) and a European demographic model that was fit to patterns of European genomic diversity (Gravel et al., 2011). For models that include a shift in the optimal trait value, we considered a relatively modest change (denoted $\Delta\phi$) equal to 2 standard deviations of the trait distribution. For reference, this would correspond to approximately a five-inch change in mean height (Fryar et al., 2016). The remaining model parameters for the simulations in Fig. 1 are given in the Supplemental Information. To compute the mean effect size $\bar{\beta}$ (Fig. 1D), we grouped alleles into 1% frequency bins and computed the mean effect size across all alleles within the bin.

When there is a bias towards trait-decreasing alleles and stabilizing selection acts on the trait, alleles at low frequencies have strongly negative effect sizes, which generates a positive correlation between effect size and frequency (Fig. 1D, red curves). When the optimal value of the phenotype increases in response to an environmental shift, the relationship between effect size and selection coefficient also transiently changes (Fig. 1B), driving some alleles with beneficial effects to higher frequencies (Fig. 1D, yellow, green, and orange curves). This effect transiently changes the relationship between allele frequency and effect size by promoting trait-increasing alleles to higher frequencies, generally increasing $\bar{\beta}$ at all frequencies. Although $\bar{\beta}$ is always negative at low frequencies for the particular parameter combinations we investigated here, at high frequencies $\bar{\beta}$ can become positive due to the preferential increase in frequency of trait-increasing alleles. These effects decay as the time since the shift event increases (Fig. 1D). The slow decay indicates that such patterns might be detectable in trait data for tens of thousands of years, with

the time-scale for detection depending on the model parameters and the precision of effect size estimates.

A statistical test for polygenic selection and mutational bias on oriented GWAS. Selection and mutational bias change the relationship between $\bar{\beta}$ and DAF (Fig. 1; Figs. S1-S3). We desire a simple statistic that will differ from zero when selection and/or mutational bias act. We first consider the integral of the area under a βDAF plot, noting that while other statistics are also likely to be informative (Yang et al., 2015), not all choices will be robust to ancestral state uncertainty (see Supplemental Information). We approximate this integral with the sum (S_β) over $\overline{\beta}$ for allele frequency bins of some width y_w.

$$S_\beta(f_i, f_j) = \sum_{y \in Y_{ij}} \overline{\beta}(y). \tag{1}$$

As in Fig. 1, we group alleles into frequency bins of width y_w such that the set Y is given by the sequence of frequency tuples $Y = \langle (0, y_w), (y_w, 2y_w), \ldots (1-y_w, 1) \rangle$. Y_{ij} refers to the subsequence of Y that includes all elements indexed between i and j, and f_i is the lower frequency in the i-th tuple while f_j is the higher frequency in the j-th tuple. We choose $y_w = 0.01$ such that there are a large number of alleles within each bin, unless otherwise noted.

We investigated how stabilizing selection with shifts in the fitness optimum are captured by $S_\beta(0, x)$ as a function of DAF x using forward simulations. When stabilizing selection acts on a trait with $\delta < 0.5$, $S_\beta(0, x)$ is negative at all x, and decreases as a function of frequency (red curve, Fig. 1E; we show in the Supplemental Information that this same pattern holds under a well-studied directional selection model for complex traits (Eyre-Walker, 2010)). When shifts in the optimum occur, higher frequency variants have mean positive effect sizes, causing $S_\beta(0, x)$ to be non-monotonic and $S_\beta(0, 1)$ to potentially have positive sign. As time elapses since the shift, the high frequency trait-increasing alleles will tend to drift to the boundary and fix or be lost, causing this signal to gradually disappear (Fig. 1E). Note that mutational bias in the absence of selection can generate a non-zero S_β – however, mutational bias alone induces $S_\beta(0, x)$ to increase in magnitude monotonically and linearly in x, a pattern that is not expected for selection. We use model-based analyses to tease apart mutational bias and selection effects in later sections.

A permutation procedure to generate a null distribution. While it is clear that S_β has non-0 expectation under the neutral null without mutational bias, the variance of S_β depends on linkage between causal alleles and non-causals. To control for potential confounding by LD, we developed a simple permutation-based procedure for computing the null-distribution of frequency-effect size relationships in GWAS summary statistics under a neutral evolutionary model. We first polarize all alleles such that the derived allele is the causal allele. Then, for each of 1,703 previously identified approximately independent linkage blocks (Berisa and Pickrell, 2016), we select a random sign (positive or negative with equal proba-

bility), and multiply all the effect sizes in the LD block by this sign. We then recompute the test statistic of interest, such as the correlation between frequency and MAF, on the randomized data. This generates a null distribution for the test statistic that conservatively accounts for the linkage between inferred effect sizes, and maintains the frequency spectrum and marginal distribution of the magnitude of inferred effect sizes. We name this framework PASTEL, or Polygenic Ancestral Selection Tests Encompassing Linkage.

Application to GWAS summary data. We applied S_β within the PASTEL framework to GWAS summary data for BMI, height (Wood et al., 2014), and educational attainment (Okbay et al., 2016) to assess its power for detecting selection, given that previous studies have suggested that these phenotypes may be under selection (Turchin et al., 2012; Berg and Coop, 2014; Robinson et al., 2015; Field et al., 2016; Racimo et al., 2018). We observe that effect sizes are correlated with frequency, and that S_β is a non-monotonic function of frequency (Fig. 2), consistent with selection and mutational bias (Fig. 1E; note that the large spike in both BMI and height at high frequency can be explained by ancestral uncertainty (Fig. S7)). We reject the neutral null for all three traits (p <5e-4; Fig. 2 & Tab. 1). We then applied our method to six additional phenotypes, which we selected to span a wide range of phenotypes that we hypothesized might be targets of selection, including body size (Wood et al., 2014), psychiatric conditions (CDG Psychiatric Genomics Consortium, 2013), immune-related traits (Franke et al., 2010), reproductive traits (Day et al., 2015), and cardiovascular traits (Global Lipids Genetics Consortium et al., 2013). We find an additional selection signal for Crohn's disease, and a marginally significant signal for schizophrenia that narrowly missed a multiple testing correction (Tab. 1 & Figs. S9-17). When including only common variants in the test, we find that seven of nine phenotypes have p-values under 0.1, suggesting strong enrichment for selected traits among the test set despite failure for some of the tests to exceed a multiple testing correction (binomial p-value 8.2×10^{-8}).

Evolutionary models for selection on human traits. While our results show that S_β has a strong non-neutral signature for five of the nine phenotypes, we sought to further understand the evolutionary models that could explain these signals. Purifying selection alone seems an unlikely candidate for most of the phenotypes, because the sign of S_β is always the same as the sign of $\bar{\beta}$ under a purifying selection model, a pattern violated by height, BMI, Crohn's, and educational attainment. Models of directional selection for increased or decreased phenotype values in the absence of mutational bias also share this pattern, as do models of mutational bias in the absence of selection (see Supplemental Information).

We hypothesized that these signals could be explained by a model of stabilizing selection, mutational bias, and shifts in the trait value conferring optimal fitness. We developed an evolutionary inference procedure based on rejection sampling (Tavaré et al., 1997) to infer the parameters that best fit the relationship between frequency and effect size that we observe in the data (see Supplemental Informa-

tion). Briefly, we calculate $S_\beta(0.01, x)$ (scaled by $S_\beta(0.01, 0.99)$) for a range of derived allele frequencies x, which we then use as summary statistics for rejection sampling. We remove the lowest frequency variants (*i.e.*, those with $x < 0.01$) for the purpose of this inference to avoid the potential impact of rare variant stratification on our results. We validated our method with extensive simulations, and found that it is an excellent estimator of the direction of both mutational bias and shift in optimal trait value (Fig. 3C&D), and a noisy estimator of the magnitude of these parameters (Fig. 3A&B). Other parameters of the model (including heritability, polygenicity, effect size distribution, and the time of the shift in the fitness landscape; see Supplemental Information for details) were inferred with low accuracy, and are not reported.

We find strong posterior support for a shift in optimal trait value ($\Delta\phi$, measured in units of standard deviations of the population trait distribution) for all five phenotypes, as well as strong signals of mutational bias (δ). Data for height and educational attainment supported a shift towards increased trait values and a mutational bias towards mutations that decrease the phenotype, while Crohn's disease and BMI supported shifts towards lower trait values and mutational bias towards trait-increasing alleles (*i.e.*, risk-increasing for Crohn's). Schizophrenia data supported a shift towards lower risk, and a bias towards protective mutations, although a substantial minority of parameter estimates supported no mutational bias or a bias in the opposite direction (Fig. 3E). To further validate these findings, we resampled from the inferred parameter distributions and performed an independent set of forward simulations. We find that the summary statistics computed on these out-of-sample simulations (which were not used to fit the data) match the trends observed in our data, confirming that the modeling framework is capable of explaining the signals we observe in the data (Fig. 3G).

Neanderthal polarization and alternate summary statistics. Although we have highlighted the ancestral/derived polarization, other polarizations, such as Neanderthal vs ancestral human alleles, can also provide insight into evolutionary processes. Recent evidence suggests that Neanderthal immune-related variants and expression-altering variants were likely targets of selection (Quach et al., 2016; Nédélec et al., 2016; McCoy et al., 2017), and some Neanderthal variants are likely to alter complex traits (Simonti et al., 2016), but little is known about polygenic selection on trait-altering Neanderthal alleles. If Neanderthals were "pre-adapted" to Europe, alleles that were fixed in Neanderthals may have accelerated the adaptation of modern humans to the European environment when admixed into humans (Enard and Petrov, 2017). Hence, we hypothesized that we may observe signals in S_β if Neanderthal alleles were systematically biased in one direction than the other, or if selection acted to promote or remove Neanderthal alleles with specific phenotypic effects once admixed into modern humans.

We tested this hypothesis by computing S_β on Neanderthal alleles that were included in previous

GWAS. The alleles were identified with the S^* statistic (Plagnol and Wall, 2006) and allele sharing with Neanderthal genomes, and hence do not suffer from the same potential biases from ancestral uncertainty as the derived/ancestral polarization. We performed both a common allele test (S_β(0.05,0.25)) and an all allele test (S_β(0,0.25)) for each of the nine phenotypes. We exclude alleles above frequency 0.25 because the vast majority of Neanderthal alleles have frequencies below 0.25.

Across the nine phenotypes we studied, we found strong signals for both height (p <5e-4) and major depression (p <5e-4) (Fig. 4), and a marginally significant signal for schizophrenia that did not pass a multiple testing correction (p =0.015). The height and schizophrenia signals were strongest when including only common alleles, whereas the depression signal was driven primarily by rare alleles. The height signal suggests selection that favored Neanderthal height-increasing alleles, while the depression signal suggests that Neanderthal alleles had a large impact on depression risk, which have been preferentially pushed to low frequency by selection. The schizophrenia signal suggests selection against schizophrenia risk or a bias towards protective alleles from Neanderthals. No other phenotypes had significant p-values.

Potential confounders. Although S_β is not sensitive to confounding by ancestral uncertainty, we were concerned that these signals could potentially be explained by other confounders, such as uncorrected population stratification. While recent studies have suggested that methods to account for stratification in GWAS often over-correct (Field et al., 2016; Bulik-Sullivan et al., 2015), rare variant stratification remains especially difficult to account for in GWAS (Mathieson and McVean, 2012). We re-computed S_β on alleles with MAF> 1% and MAF> 5%, and found that the signals are robust within common alleles alone, suggesting that population structure is unlikely to confound our estimates (Fig S9-17 and Tab. 1). In addition, we computed the βDAF curve for subsets of SNPs that are minimally differentiated between northern and southern Europe. There is a known gradient of height from south to north in Europe (Turchin et al., 2012), so if the signals we observe were confounded by population stratification, we would expect to see a flatter βDAF curve for less geographically differentiated SNPs at which little differentiation in frequency exists between these regions. In contrast, we observe a pattern that is concordant across all subsets of SNPS regardless of the frequency difference between northern and southern Europe (Fig. S7). Lastly, we recomputed S_β on GWAS from the UK Biobank for our top three signals as a replication cohort that employed strict population structure control. We confirm the signal for both educational attainment and BMI (Fig. S18). Interestingly, height was not replicated. We also applied two previous approaches that detected signals of selection acting on height when analyzing the GIANT summary statistics and found that neither of these replicated in the UKBB (Fig. S6) (Turchin et al., 2012; Yang et al., 2015). These results are consistent with either over-correction of structure within the UKBB or under-correction in the GIANT data (see Discussion).

Discussion

Many studies have suggested that selection shapes human genetic variation (Enard et al., 2014), and it has long been theorized that it drives some of the variance in a broad range of human complex phenotypes (Hernandez et al., 2011). Here, we developed a novel empirical framework (PASTEL) and rejection sampling approach for detecting polygenic selection and mutational bias that can be applied to GWAS summary data for a single population. Our approach can capture relatively ancient selection events, and retains power when applied only to common alleles, for which it is more straightforward to correct for population stratification. We call this approach an "evolutionary compass", because orienting alleles by their ancestral/derived or modern human/Neanderthal status within our framework provides insight into the evolutionary processes shaping complex traits. We applied this evolutionary compass to GWAS summary data for nine phenotypes, and showed that five of them (educational attainment, height, Crohn's disease, BMI, and schizophrenia) suggest a role for selection in shaping trait variation. It has been previously suggested that height (Turchin et al., 2012; Berg and Coop, 2014; Robinson et al., 2015; Yang et al., 2015) and BMI are under selection (Yang et al., 2015), but studies have reported both polygenic adaptation and widespread negative selection as possible selection mechanisms. Our results are consistent with a shift towards higher optimal trait values of educational attainment and height, but lower optimal trait values for BMI, schizophrenia, Crohn's disease risk, suggesting that long-term stabilizing selection on these traits has been punctuated with periods of polygenic adaptation.

If selection acts on biomedically relevant complex traits in humans such as Crohn's disease and schizophrenia, there are important implications for the future of both medical and evolutionary genomics. In medical genomics, an ongoing debate about the genomic architecture of complex diseases is at the forefront of the field (Manolio et al., 2009). When strong selection acts on complex traits, it can elevate the role of rare alleles in driving trait variance (Lohmueller, 2014). If rare alleles contribute a larger fraction of the genetic variance than is expected under neutral models, then very large GWAS that use only array-based genotyping information are very unlikely to be able to capture these signals, and sequence-based studies and powerful rare variant approaches that are robust to evolutionary forces (including those not investigated here, such as partial recessivity) will be needed (Uricchio et al., 2016; Sanjak et al., 2017a; Hernandez et al., 2017). Moreover, recent work has suggested that the over-representation of Europeans in GWAS has limited the effectiveness of estimating polygenic risk scores in other human populations (Martin et al., 2017). This is problematic for the transfer of genomic research into the clinic, where precision medicine initiatives relying on personal genetic information will be most successful if genetic risk can be accurately inferred in diverse populations. While this effect could be attributed to neutral

demographic forces, if selection has driven numerous phenotypes to acclimate to local environmental conditions in ancestral human populations worldwide it could exacerbate this problem dramatically.

In the field of evolutionary genomics, most studies have agreed that the impact of selection is widespread on the human genome, but the evolutionary mechanisms that drive genetic and phenotypic diversity have been widely debated (Hernandez et al., 2011; Enard et al., 2014). In our study, we showed that the selection signals in Europeans for BMI and Crohn's disease are consistent with a bias in mutation rate towards trait-increasing alleles, and a shift to a lower optimal value of the trait, while height and educational attainment are consistent with a mutational bias towards trait-increasing alleles and a shift towards higher values of the trait optimum. The signal for schizophrenia is consistent with an ancestral shift towards a lower optimum and a stabilizing selection, with or without a mutational bias. It should be noted that the model we used to fit these data assumed no more than one shift in the optimal phenotype value, whereas this quantity is likely to vary continuously with environmental conditions. Models that additionally account for sexual dimorphism (Stulp and Barrett, 2016), higher dimensional trait spaces (Simons et al., 2018), and evolutionary history of multiple populations (Berg and Coop, 2014; Racimo et al., 2018) may be required to better understand the generality of these results across human populations and traits.

Neanderthal introgression into modern humans has played an important role in shaping traits in non-African populations (Wall et al., 2013; McCoy et al., 2017). Given that Neanderthal alleles may contribute disproportionately to the genetic variance in some traits (Simonti et al., 2016) and that some high frequency trait-associated alleles have Neanderthal origins (Dannemann and Kelso, 2017; Prüfer et al., 2017), we hypothesized that Neanderthal alleles for traits under selection might show distinct patterns from modern human alleles. Although Neanderthal alleles do not share a common demographic history with modern human alleles, under the neutral null hypothesis we do not expect Neanderthal alleles to have an increasing or decreasing frequency/effect-size relationship, or to have a distribution that differs substantially from modern human alleles. We therefore computed S_β on alleles that have a Neanderthal origin. Alleles for height and depression show strikingly different patterns than alleles with modern human origins. Our results for height can be explained by selection to promote Neanderthal height-increasing alleles to high frequency, either along the Neanderthal lineage predating human introgression, or after admixture with human populations. In contrast, our results for depression risk are consistent with an excess of depression risk from Neanderthals (Simonti et al., 2016), and selection preferentially driving large effect alleles to low frequency.

Inference of selection on complex traits is vulnerable to several possible confounders, including population stratification and pleiotropic selection on off-target phenotypes (Novembre and Barton, 2018).

Although theory suggests that stratification should be straightforward to detect and correct at high frequency variants in large samples (Patterson et al., 2006), an uncorrected bias in the inferred β values due to population structure can make our test (as well most others, such as Berg and Coop (2014); Yang et al. (2015); Field et al. (2016); Berg et al. (2017); Racimo et al. (2018)) anti-conservative. We used a series of experiments to show that population structure is unlikely to bias the majority of our results, including showing that the signal is robust to the exclusion of rare alleles, dissecting our signal as a function of allele frequency differentiation within Europe, and replicating in an outside cohort. However, one of our strongest signals (height) did not replicate the UK Biobank, while two other signals of selection form earlier height studies also did not replicate in the UK Biobank (Turchin et al., 2012; Yang et al., 2015).

The most conservative interpretation of the non-replication of height is to suppose that the some of the signals we and others observed in the GIANT cohort are driven by population structure, and the UK Biobank analysis correctly removes this signal. Indeed, LD score regression on height GWAS data is consistent with a moderate amount of residual uncorrected population structure (Bulik-Sullivan et al., 2015), but inflation in the relevant test statistic can be driven by selection, population structure, or high polygenicity (Bulik-Sullivan et al., 2015; Loh et al., 2017). An alternative explanation to stratification in GIANT is that PCA-based population structure corrections tend to over-correct (Field et al., 2016). If selection on highly polygenic height variation is a substantial contributor to allele frequency differentiation within Europe, it could cause height-altering alleles to be disproportionately ancestry informative and induce bias in effect size estimates (Bhatia et al., 2016). This effect should be modest for alleles with large effects and traits with low polygenicity, for which most alleles are unlikely to be informative about trait values, but it has been suggested that a preponderance of the human genome is informative about height variation (Field et al., 2016; Boyle et al., 2017). Further research is needed to better disentanlge stratification and selection, and some caution in interpreting the results of polygenic selection tests is warranted while this field develops (Novembre and Barton, 2018).

Pleiotropy can also induce biases in complex trait selection detection. Selection on traits with a shared genomic basis and correlated effect sizes could result in false positives, where a trait that is not the selection target is spuriously identified. This is a general limitation of most complex trait selection methods (but see Berg et al. (2017); Simons et al. (2018)). This phenomenon is clearly highlighted by our results on educational attainment, a phenotype which did not exist until very recent times. While it would be tempting to identify intelligence as the target of selection here, it is possible that any (unknown) trait with a shared genetic basis and correlated effect sizes could be the target. This remains a major problem in detecting and interpreting selection signals on complex traits.

Among the nine traits that we tested, we found that five had strong signals of polygenic selection, and

seven of the nine had marginal evidence for non-neutrality. However, this does not imply that the others are not under selection. The power of our test depends on the strength of selection, the polygenicity of the trait, the heritability of the trait, and the mutational bias, in addition to the size of the GWAS. If a trait is under strong stabilizing selection, but the mutation rate of trait-increasing and -decreasing alleles is exactly equal, then our test has no power. Moreover, if selection is weak, a small number of causal alleles drive variance in the trait, or the trait is only weakly heritable, power is greatly diminished. However, increased sample sizes in GWAS will increase our power, because the variance on effect size estimates for even weak effect causal alleles decreases with sample size. In addition to working directly on GWAS summary statistics from a single population, one strength of our permutation-based approach is that other informative statistics, such as the absolute value of the deviation between ancestral and derived effect sizes, could also easily be applied, and may have higher power. In future studies, it will be advantageous to apply and compare other summary statistics, and to use the information in such summary statistics to improve the inference of evolutionary parameters such as the timing of shifts in the trait optima and the strength of selection.

Acknowledgments

The authors acknowledge the support of NIGMS grant K12GM088033 and the Stanford IRACDA program (LHU) and thank Noah Rosenberg, Jeremy Berg, Doc Edge, Graham Coop, and Josh Akey for comments that substantially improved the manuscript. We also thank Jonathan Pritchard, Arbel Harpak, Yair Field, Ziyue Gao, and members of the Rosenberg, Coop, and Pritchard labs for helpful comments, as well as Josh Akey and Rajiv McCoy for providing a list of inferred Neanderthal alleles.

References

Barton, N. (1986). The maintenance of polygenic variation through a balance between mutation and stabilizing selection. Genetics Research *47*, 209–216.

Berg, J. J. and Coop, G. (2014). A population genetic signal of polygenic adaptation. PLoS Genetics *10*, e1004412.

Berg, J. J., Zhang, X. and Coop, G. (2017). Polygenic Adaptation has Impacted Multiple Anthropometric Traits. bioRxiv , 167551.

Berisa, T. and Pickrell, J. K. (2016). Approximately independent linkage disequilibrium blocks in human populations. Bioinformatics (Oxford, England) *32*, 283–285.

Bhatia, G., Furlotte, N. A., Loh, P.-R., Liu, X., Finucane, H. K., Gusev, A. and Price, A. (2016). Correcting subtle stratification in summary association statistics. bioRxiv , 076133.

Boyle, E. A., Li, Y. I. and Pritchard, J. K. (2017). An expanded view of complex traits: from polygenic to omnigenic. Cell *169*, 1177–1186.

Bulik-Sullivan, B. K., Loh, P.-R., Finucane, H. K., Ripke, S., Yang, J., Patterson, N., Daly, M. J., Price, A. L., Neale, B. M., of the Psychiatric Genomics Consortium, S. W. G. et al. (2015). LD Score regression distinguishes confounding from polygenicity in genome-wide association studies. Nature Genetics *47*, 291–295.

Charlesworth, B. (2013). Stabilizing selection, purifying selection, and mutational bias in finite populations. Genetics *194*, 955–971.

Dannemann, M. and Kelso, J. (2017). The Contribution of Neanderthals to Phenotypic Variation in Modern Humans. The American Journal of Human Genetics *101*, 578–589.

Day, F. R., Ruth, K. S., Thompson, D. J., Lunetta, K. L., Pervjakova, N., Chasman, D. I., Stolk, L., Finucane, H. K., Sulem, P., Bulik-Sullivan, B. et al. (2015). Large-scale genomic analyses link reproductive aging to hypothalamic signaling, breast cancer susceptibility and BRCA1-mediated DNA repair. Nature Genetics *47*, 1294–1303.

Enard, D., Messer, P. W. and Petrov, D. A. (2014). Genome-wide signals of positive selection in human evolution. Genome Research *24*, 885–895.

Enard, D. and Petrov, D. A. (2017). RNA viruses drove adaptive introgressions between Neanderthals and modern humans. bioRxiv , 120477.

Eyre-Walker, A. (2010). Genetic architecture of a complex trait and its implications for fitness and genome-wide association studies. Proceedings of the National Academy of Sciences *107*, 1752–1756.

Field, Y., Boyle, E. A., Telis, N., Gao, Z., Gaulton, K. J., Golan, D., Yengo, L., Rocheleau, G., Froguel, P., McCarthy, M. I. et al. (2016). Detection of human adaptation during the past 2000 years. Science *354*, 760–764.

Franke, A., McGovern, D. P., Barrett, J. C., Wang, K., Radford-Smith, G. L., Ahmad, T., Lees, C. W., Balschun, T., Lee, J., Roberts, R. et al. (2010). Genome-wide meta-analysis increases to 71 the number of confirmed Crohn's disease susceptibility loci. Nature Genetics *42*, 1118–1125.

Fryar, C. D., Gu, Q., Ogden, C. L. and Flegal, K. M. (2016). Anthropometric Reference Data for Children and Adults: United States, 2011-2014. Vital health statistics. Series 3, Analytical and epidemiological studies , 1.

Gazal, S., Finucane, H., Furlotte, N. A., Loh, P.-R., Palamara, P. F., Liu, X., Schoech, A., Bulik-Sullivan, B., Neale, B. M., Gusev, A. et al. (2017). Linkage disequilibrium dependent architecture of human complex traits reveals action of negative selection. bioRxiv , 082024.

Gilad, Y., Oshlack, A. and Rifkin, S. A. (2006). Natural selection on gene expression. Trends in Genetics *22*, 456–461.

Gravel, S., Henn, B. M., Gutenkunst, R. N., Indap, A. R., Marth, G. T., Clark, A. G., Yu, F., Gibbs, R. A., Bustamante, C. D., Altshuler, D. L. et al. (2011). Demographic history and rare allele sharing among human populations. Proceedings of the National Academy of Sciences *108*, 11983–11988.

Hernandez, R. D. (2008). A flexible forward simulator for populations subject to selection and demography. Bioinformatics *24*, 2786–2787.

Hernandez, R. D., Kelley, J. L., Elyashiv, E., Melton, S., Auton, A., McVean, G., Sella, G., Przeworski, M. et al. (2011). Classic selective sweeps were rare in recent human evolution. Science *331*, 920–924.

Hernandez, R. D., Uricchio, L. H., Hartman, K., Ye, J., Dahl, A. and Zaitlen, N. (2017). Singleton Variants Dominate the Genetic Architecture of Human Gene Expression. bioRxiv , 219238.

Jain, K. and Stephan, W. (2017). Rapid adaptation of a polygenic trait after a sudden environmental shift. Genetics *206*, 389–406.

Locke, A. E., Kahali, B., Berndt, S. I., Justice, A. E., Pers, T. H., Day, F. R., Powell, C., Vedantam, S., Buchkovich, M. L., Yang, J. et al. (2015). Genetic studies of body mass index yield new insights for obesity biology. Nature *518*, 197–206.

Loh, P.-R., Kichaev, G., Gazal, S., Schoech, A. P. and Price, A. L. (2017). Mixed model association for biobank-scale data sets. bioRxiv , 194944.

Lohmueller, K. E. (2014). The impact of population demography and selection on the genetic architecture of complex traits. PLoS Genetics *10*, e1004379.

Manolio, T. A., Collins, F. S., Cox, N. J., Goldstein, D. B., Hindorff, L. A., Hunter, D. J., McCarthy, M. I., Ramos, E. M., Cardon, L. R., Chakravarti, A. et al. (2009). Finding the missing heritability of complex diseases. Nature *461*, 747–753.

Martin, A. R., Gignoux, C. R., Walters, R. K., Wojcik, G. L., Neale, B. M., Gravel, S., Daly, M. J., Bustamante, C. D. and Kenny, E. E. (2017). Human demographic history impacts genetic risk prediction across diverse populations. The American Journal of Human Genetics *100*, 635–649.

Mathieson, I. and McVean, G. (2012). Differential confounding of rare and common variants in spatially structured populations. Nature Genetics *44*, 243–246.

McCoy, R. C., Wakefield, J. and Akey, J. M. (2017). Impacts of Neanderthal-introgressed sequences on the landscape of human gene expression. Cell *168*, 916–927.

Messer, P. W. and Petrov, D. A. (2013). Population genomics of rapid adaptation by soft selective sweeps. Trends in Ecology & Evolution *28*, 659–669.

Nédélec, Y., Sanz, J., Baharian, G., Szpiech, Z. A., Pacis, A., Dumaine, A., Grenier, J.-C., Freiman, A., Sams, A. J., Hebert, S. et al. (2016). Genetic ancestry and natural selection drive population differences in immune responses to pathogens. Cell *167*, 657–669.

Novembre, J. and Barton, N. H. (2018). Tread Lightly Interpreting Polygenic Tests of Selection. Genetics *208*, 1351–1355.

Okbay, A., Beauchamp, J. P., Fontana, M. A., Lee, J. J., Pers, T. H., Rietveld, C. A., Turley, P., Chen, G.-B., Emilsson, V., Meddens, S. F. W. et al. (2016). Genome-wide association study identifies 74 loci associated with educational attainment. Nature *533*, 539–542.

Patterson, N., Price, A. L. and Reich, D. (2006). Population structure and eigenanalysis. PLoS genetics *2*, e190.

Plagnol, V. and Wall, J. D. (2006). Possible ancestral structure in human populations. PLoS genetics *2*, e105.

Pritchard, J. K., Pickrell, J. K. and Coop, G. (2010). The genetics of human adaptation: hard sweeps, soft sweeps, and polygenic adaptation. Current Biology *20*, R208–R215.

Prüfer, K., de Filippo, C., Grote, S., Mafessoni, F., Korlević, P., Hajdinjak, M., Vernot, B., Skov, L., Hsieh, P., Peyrégne, S. et al. (2017). A high-coverage Neandertal genome from Vindija Cave in Croatia. Science , eaao1887.

Quach, H., Rotival, M., Pothlichet, J., Loh, Y.-H. E., Dannemann, M., Zidane, N., Laval, G., Patin, E., Harmant, C., Lopez, M. et al. (2016). Genetic adaptation and neandertal admixture shaped the immune system of human populations. Cell *167*, 643–656.

Racimo, F., Berg, J. J. and Pickrell, J. K. (2018). Detecting polygenic adaptation in admixture graphs. Genetics *208*, 1565–1584.

Robertson, A. (1956). The effect of selection against extreme deviants based on deviation or on homozygosis. Journal of Genetics *54*, 236–248.

Robinson, M. R., Hemani, G., Medina-Gomez, C., Mezzavilla, M., Esko, T., Shakhbazov, K., Powell, J. E., Vinkhuyzen, A., Berndt, S. I., Gustafsson, S. et al. (2015). Population genetic differentiation of height and body mass index across Europe. Nature Genetics *47*, 1357–1362.

Sabeti, P. C., Reich, D. E., Higgins, J. M., Levine, H. Z., Richter, D. J., Schaffner, S. F., Gabriel, S. B., Platko, J. V., Patterson, N. J., McDonald, G. J. et al. (2002). Detecting recent positive selection in the human genome from haplotype structure. Nature *419*, 832–837.

Sabeti, P. C., Schaffner, S. F., Fry, B., Lohmueller, J., Varilly, P., Shamovsky, O., Palma, A., Mikkelsen, T., Altshuler, D. and Lander, E. (2006). Positive natural selection in the human lineage. Science *312*, 1614–1620.

Sanjak, J. S., Long, A. D. and Thornton, K. R. (2017a). A model of compound heterozygous, loss-of-function alleles is broadly consistent with observations from complex-disease GWAS datasets. PLoS Genetics *13*, e1006573.

Sanjak, J. S., Sidorenko, J., Robinson, M. R., Thornton, K. R. and Visscher, P. M. (2017b). Evidence of directional and stabilizing selection in contemporary humans. Proceedings of the National Academy of Sciences , 201707227.

Schoech, A., Jordan, D., Loh, P.-R., Gazal, S., O'Connor, L., Balick, D. J., Palamara, P. F., Finucane, H., Sunyaev, S. R. and Price, A. L. (2017). Quantification of frequency-dependent genetic architectures and action of negative selection in 25 UK Biobank traits. bioRxiv , 188086.

Shungin, D., Winkler, T. W., Croteau-Chonka, D. C., Ferreira, T., Locke, A. E., Mägi, R., Strawbridge, R. J., Pers, T. H., Fischer, K., Justice, A. E. et al. (2015). New genetic loci link adipose and insulin biology to body fat distribution. Nature *518*, 187–196.

Simons, Y. B., Bullaughey, K., Hudson, R. R. and Sella, G. (2018). A population genetic interpretation of GWAS findings for human quantitative traits. PLoS biology *16*, e2002985.

Simonti, C. N., Vernot, B., Bastarache, L., Bottinger, E., Carrell, D. S., Chisholm, R. L., Crosslin, D. R., Hebbring, S. J., Jarvik, G. P., Kullo, I. J. et al. (2016). The phenotypic legacy of admixture between modern humans and Neandertals. Science *351*, 737–741.

Stulp, G. and Barrett, L. (2016). Evolutionary perspectives on human height variation. Biological Reviews *91*, 206–234.

Tavaré, S., Balding, D. J., Griffiths, R. C. and Donnelly, P. (1997). Inferring coalescence times from DNA sequence data. Genetics *145*, 505–518.

CDG Psychiatric Genomics Consortium (2013). Identification of risk loci with shared effects on five major psychiatric disorders: a genome-wide analysis. The Lancet *381*, 1371–1379.

Global Lipids Genetics Consortium et al. (2013). Discovery and refinement of loci associated with lipid levels. Nature Genetics *45*, 1274–1283.

Thousand Genomes Project Consortium et al. (2015). A global reference for human genetic variation. Nature *526*, 68–74.

Torgerson, D. G., Boyko, A. R., Hernandez, R. D., Indap, A., Hu, X., White, T. J., Sninsky, J. J., Cargill, M., Adams, M. D., Bustamante, C. D. et al. (2009). Evolutionary processes acting on candidate cis-regulatory regions in humans inferred from patterns of polymorphism and divergence. PLoS Genetics *5*, e1000592.

Turchin, M. C., Chiang, C. W., Palmer, C. D., Sankararaman, S., Reich, D., Hirschhorn, J. N., of ANthropometric Traits (GIANT) Consortium, G. I. et al. (2012). Evidence of widespread selection on standing variation in Europe at height-associated SNPs. Nature Genetics *44*, 1015–1019.

Uricchio, L. H., Zaitlen, N. A., Ye, C. J., Witte, J. S. and Hernandez, R. D. (2016). Selection and explosive growth alter genetic architecture and hamper the detection of causal rare variants. Genome Research *26*, 863–873.

Voight, B. F., Kudaravalli, S., Wen, X. and Pritchard, J. K. (2006). A map of recent positive selection in the human genome. PLoS Biology *4*, e72.

Wall, J. D., Yang, M. A., Jay, F., Kim, S. K., Durand, E. Y., Stevison, L. S., Gignoux, C., Woerner, A., Hammer, M. F. and Slatkin, M. (2013). Higher levels of Neanderthal ancestry in East Asians than in Europeans. Genetics *194*, 199–209.

Wood, A. R., Esko, T., Yang, J., Vedantam, S., Pers, T. H., Gustafsson, S., Chu, A. Y., Estrada, K., Luan, J., Kutalik, Z. et al. (2014). Defining the role of common variation in the genomic and biological architecture of adult human height. Nature Genetics *46*, 1173–1186.

Yang, J., Bakshi, A., Zhu, Z., Hemani, G., Vinkhuyzen, A. A., Lee, S. H., Robinson, M. R., Perry, J. R., Nolte, I. M., van Vliet-Ostaptchouk, J. V. et al. (2015). Genetic variance estimation with imputed variants finds negligible missing heritability for human height and body mass index. Nature Genetics *47*, 1114–1120.

Zeng, J., de Vlaming, R., Wu, Y., Robinson, M., Lloyd-Jones, L., Yengo, L., Yap, C., Xue, A., Sidorenko, J., McRae, A. et al. (2018). Signatures of negative selection in the genetic architecture of human complex traits. Nature Genetics *To appear*.

Figures & Tables

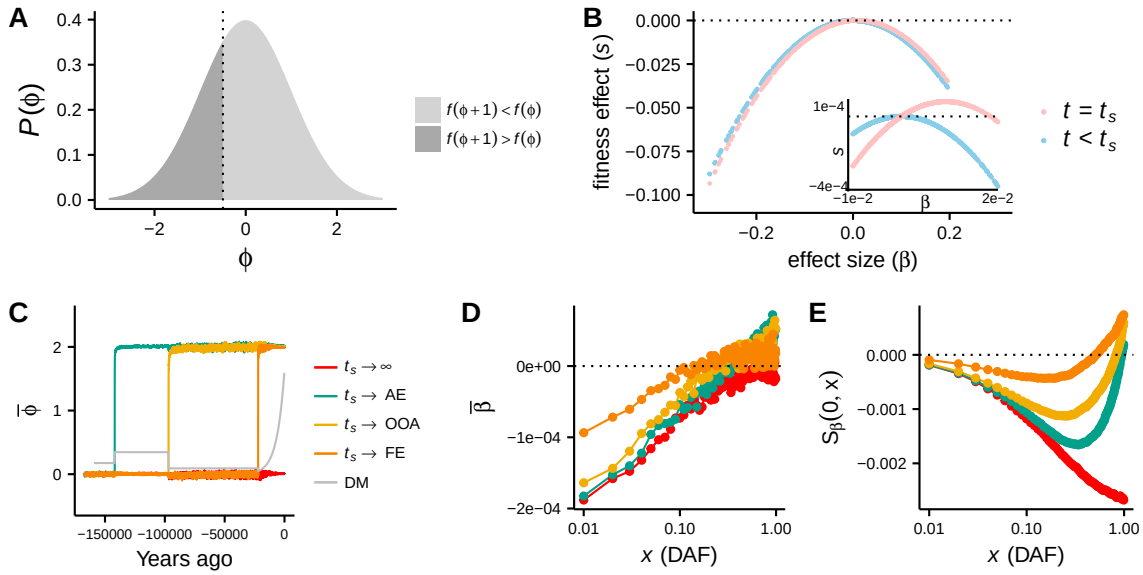

Figure 1: Panels A-B are schematics of the trait model, while C-E show simulation results. A: fitness impact of a $\beta = 1$ mutation. At equilibrium, the trait distribution $P(\phi)$ is symmetric about the optimal value of the phenotype, $\phi = 0$. Individuals with $\phi < -\frac{1}{2}$ would increase in fitness ($f(\phi+1) > f(\phi)$), shaded dark gray) given a mutation with $\beta = 1$, while all others decrease in fitness. B: schematic of the relationship between effect size and fitness effect. At time $t = t_s$, the optimal trait value ϕ_o increases, and trait-decreasing alleles have decreased fitness while trait-increasing alleles have increased fitness. Still, only trait-increasing alleles of small effect are on average fitness-increasing (inset). C. Mean trait value $\bar{\phi}$ as a function of time for four simulated trait models, differentiated by the time of a shift in selection pressure. The simulated European demographic model is plotted in the background (not to scale) D. $\bar{\beta}$ as a function of derived allele frequency (DAF) for each model simulated in C. E. $S_\beta(0, x)$ as a function of DAF for each model plotted in C. D and E represent the mean over 100 independent simulations. (Abbreviations: *AE*: ancestral expansion, *OOA*: out-of-Africa, *FE*: founding of Europe, *DM*: demographic model).

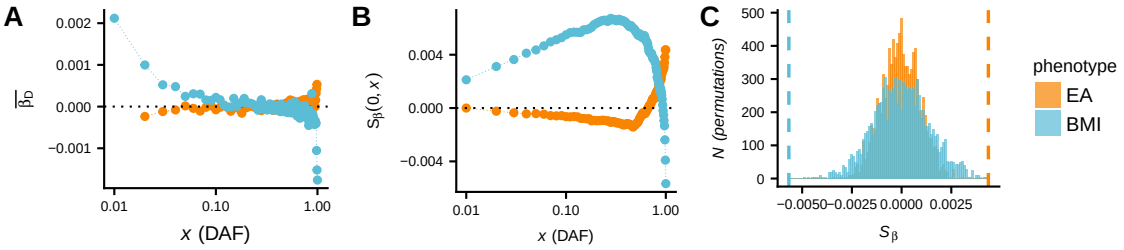

Figure 2: A: $\bar{\beta}$ as a function of DAF for BMI and educational attainment (EA). B: $S_\beta(0, x)$ for the same data. C: neutral null distribution of $S_\beta(0, 1)$ obtained by permutations in PASTEL. The vertical dashed line indicates the observed value of $S_\beta(0, 1)$ in the GWAS summary data.

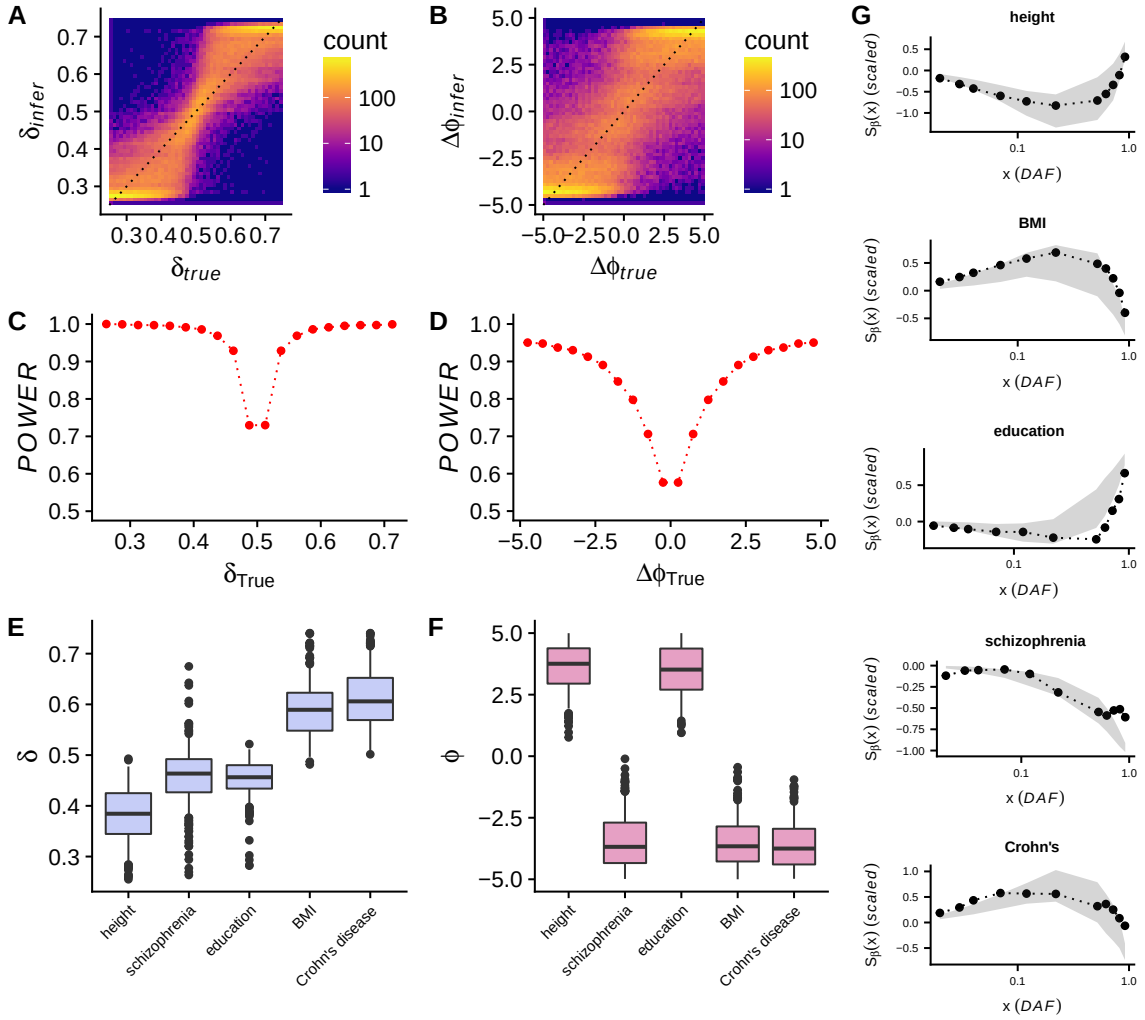

Figure 3: A-B: Inferred mutation bias (A) and selection shift (B) parameters as a function of true parameter values for our rejection sampling method. C-D: Power of our rejection sampling method to correctly identify the direction of mutation bias (C) and shift in optimal phenotype value (D), as a function of the true parameter value. E-F: Inferred approximate posterior distributions for five phenotypes identified as being under selection using PASTEL. G: Out-of-sample simulations using parameters inferred in E-F, plotted with the data used to fit each model. Gray envelopes represent the middle 50% of simulation replicates, while the black points and curves show the observed data for each phenotype.

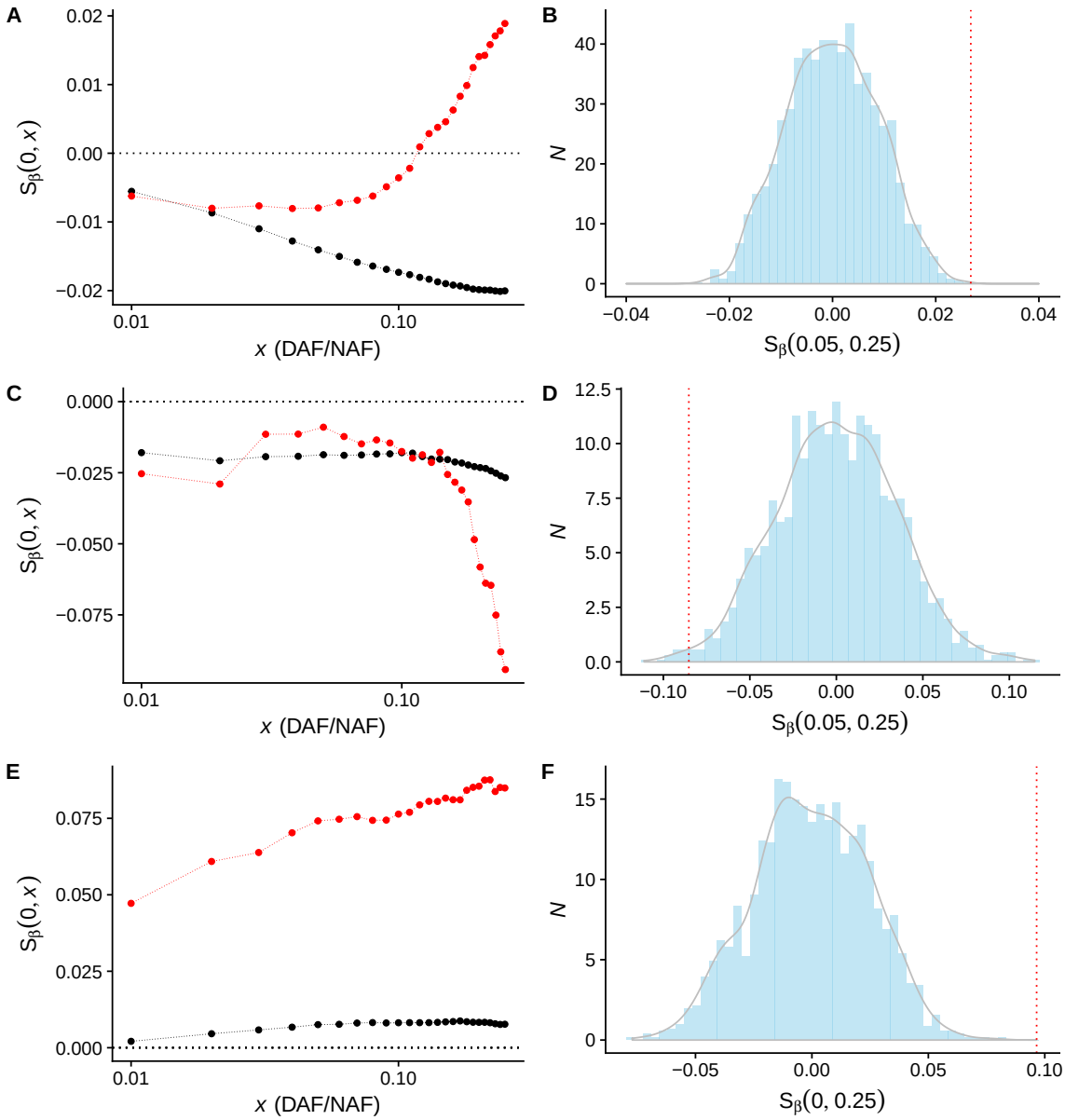

Figure 4: Signals of polygenic selection and mutation bias on Neanderthal alleles. A-B correspond to height, C-D correspond to schizophrenia, and E-F correspond to major depression. The left column shows $S_\beta(0, x)$ for Neanderthal alleles (red) and modern human alleles for comparison (truncated at allele frequency of 0.25). The right column shows $S_\beta(x_i, 0.25)$ for PASTEL-based permutations, where the observed signal is shown in the red dashed line and the value of x_i is indicated under the plot.

Phenotype	$S_\beta(0,1)$ p-value	$S_\beta(0.01,0.99)$ p-value	$S_\beta(0.05,0.95)$ p-value
Height	$< 0.0005^{**}$	$< 0.0005^{**}$	$< 0.0005^{**}$
BMI	$< 0.0005^{**}$	$< 0.0005^{**}$	$< 0.0005^{**}$
WHR-BMI	0.566	0.8325	0.341
Education	$< 0.0005^{**}$	$< 0.0005^{**}$	$< 0.0005^{**}$
GLL	0.4655	0.434	0.5645
Crohn's disease	0.0025^{**}	0.0075^{*}	0.018^{*}
Menopause onset	0.1585	0.46	0.0475^{*}
Depression	0.3915	0.01^{*}	0.0305^{*}
Schizophrenia	0.0085^{*}	0.0035^{**}	0.0625

Table 1: PASTEL-based p-values corresponding to GWAS summary statistics for nine phenotypes that we hypothesized may be under selection. Values in the first column include all alleles, while the second and third columns correspond to tests including only alleles with MAF $> 1\%$ and MAF $> 5\%$, respectively. **: Tests that pass a multiple testing correction, $p < 0.005$. *: Tests that were marginally significant ($p < 0.05$). *BMI: body mass index, WHR-BMI: waist-hip ratio adjusted for body mass index, GLL: global lipid levels*

Supplemental Information

An evolutionary compass to detect selection and mutational bias

Selection on quantitative traits is known to induce dependency between mean squared effect sizes and derived allele frequency (DAF) (Eyre-Walker, 2010; Uricchio et al., 2016), but the relationship between effect sizes $\bar{\beta}$ and DAF under selection models has not been widely explored. Under some models, for example when mutation rates for trait increasing and decreasing alleles are symmetric and the fitness cost of a mutation does not depend on the direction of its effect, selection will not induce a relationship between effect size and allele frequency. However, other models, such as those in which selection preferentially drives trait-increasing alleles to high frequency with selection pressure that increases as a function of β, may drive such a correlation (*e.g.*, Fig. S1A-C), which could potentially be detected in GWAS summary statistics data. We hypothesized that a better understanding of this relationship between β and DAF could provide new insights into the evolution of complex traits.

Models with symmetric mutation rates have often been applied to quantitative traits, but there is no *a priori* reason to suppose that this condition is met in natural populations. Indeed, it is possible that there are an unequal number of fixed bi-allelic sites genome-wide that can increase or decrease a phenotype relative to its current value, which naturally will change the relative rate of trait-increasing as compared to trait-decreasing alleles. For example, if past selection events have driven the phenotype to ever larger values, we might expect that the majority of trait-increasing alleles have already been fixed by positive selection in the evolutionary past, and that further recurrent mutations at these fixed sites would therefore decrease the phenotype.

Temporal variation in the optimal value of selected traits may also be an important determinant of the evolutionary dynamics of complex traits, as such changes may be a mechanism for polygenic adaptation (Jain and Stephan, 2017). When a population's environment is altered, perhaps by migration, a change in climate, or the elimination/introduction of competing species, it is likely that selection pressures on phenotypes will also change. If the population persists long enough in this new environment it is expected that the phenotype mean will approach the new phenotype optimum, and the population will again be at equilibrium. In the intervening time, while the population is out of equilibrium, allele frequencies will shift as a function of their effect on the phenotype. Our goal is to capture selection's impact on the causal variation during this out-of-equilibrium time period.

In this project, we sought to capture how mutational bias and selection pressure would affect the relationship between $\bar{\beta}$ and allele frequency, and to use this information in designing a statistical test to detect mutational bias and selection. In the following sections, we use analytical theory and simulations to build intuition about the relationship between these evolutionary processes and patterns that could be observed in GWAS summary statistic data.

Building intuition with the βDAF plot and S_β

To build intuition about how evolutionary parameters affect the relationship between β and DAF we performed analytical calculations and simulations of simple evolutionary models that included directional selection, stabilizing selection, and mutational bias. Throughout these calculations, we suppose that although mutation rate can be biased towards trait-increasing or trait-decreasing alleles, the distribution of trait-increasing alleles is the same as that for trait-decreasing alleles.

Mutational bias alone

Mutational bias alone (*i.e.*, in the absence of selection) does not induce a dependency between $\bar{\beta}$ and DAF because mutations with differing βs are all equally likely to reach any given frequency (Fig. S1D).

Hence, if the mutational bias is δ is the proportion of *de novo* mutations that are trait-increasing and the mean of the absolute value of a new mutation is $\mathbb{E}[|\beta|]$, then $\mathbb{E}[\beta] = \delta\mathbb{E}[|\beta|] - (1-\delta)\mathbb{E}[|\beta|]$. Note that when $\delta = 0.5$, mutation rates are symmetric, and $\mathbb{E}[\beta] = 0$.

Supposing that we decompose the frequency spectrum into k bins, when there is no selection $\mathbb{E}[S_\beta(0,1)] = \sum_{i=1}^{k} \mathbb{E}[\beta] = k\left(\delta\mathbb{E}[|\beta|] - (1-\delta)\mathbb{E}[|\beta|]\right)$. We perform this calculation for a variety of values of δ and a symmetric distribution of effect sizes, as well as stochastic simulations in which we select effect sizes randomly (Fig. S1D), and observe excellent agreement between this simple calculation (solid lines) and the simulations (points).

$\mathbb{E}[S_\beta(0,x)]$ increases monotonically and linearly in x when mutational bias acts in the absence of selection on the trait, and the sign of S_β is always equal to the direction of the mutational bias (*i.e.*, mutational bias greater than 0.5 leads to positive S_β, while mutational bias less than 0.5 leads to negative S_β).

Polygenic adaptation

We next considered a toy model in which directional polygenic adaptation acts to increase the frequency of trait-increasing alleles. We suppose that trait-increasing alleles with effect size β have selection coefficients s with $\beta = s^\tau$, and that selection coefficients are drawn from a leptokurtic Γ-distribution peaked near 0. This model (which was proposed by Eyre-Walker for traits under negative selection (Eyre-Walker, 2010)) captures the idea that many alleles will have weak effects, and hence weak selective effects, while a small portion of alleles may have strong effects on the trait and be under relatively strong selection. We further suppose that the distribution and mutation rate of trait-increasing are the same as trait-decreasing alleles. We assume that the influence of binomial sampling is small and we do not account for it.

The time-dependent dynamics of the relationship between β and derived allele frequency are complex under such a model (because they depend on the transition probabilities from every possible initial frequency to every possible final frequency for all segregating selected alleles), but we can easily solve for the equilibrium state using diffusion theory. Under this model, the equilibrium frequency spectrum (i.e., the distribution of derived allele frequencies in the population at any given time) of trait increasing alleles is given by

$$f^+_{a,b}(x) = \int_\gamma \Gamma[a,b,\gamma] e^{-2\gamma} \frac{1-e^{2\gamma(1-x)}}{(e^{-2\gamma}-1)x(1-x)} d\gamma = \left(\frac{b}{4N}\right)^a \frac{\left(-\zeta[a,\frac{b}{4N}] + \zeta[a,1-x+\frac{b}{4N}]\right)}{x(x-1)}, \tag{2}$$

where $\Gamma[a,b,\gamma] = \frac{a^b}{\Gamma(a)}\gamma^{a-1}e^{-b\gamma}$, a and b are the parameters of the Γ-distribution, ζ is the Riemann zeta function, and γ is the population-scaled selection coefficient $2Ns$. Trait-decreasing alleles have a neutral frequency spectrum, which is given by $f^-_{a,b}(x) = \frac{1}{x}$. The mean value of β for trait increasing alleles at frequency x is given by

$$\beta^+_{a,b}(x) = \int_\gamma \frac{\Gamma[a,b,\gamma]\left(\frac{\gamma}{2N}\right)^\tau e^{-2\gamma}\frac{1-e^{2\gamma(1-x)}}{(e^{-2\gamma}-1)x(1-x)}}{f_{a,b}(x)} d\gamma = \frac{(4N)^{-\tau}\Gamma[a+\tau]\left(\zeta[a+\tau,1+\frac{b}{4N}] - \zeta[a+\tau,x+\frac{b}{4N}]\right)}{\Gamma[a]\left(\zeta[a,1+\frac{b}{4N}] - \zeta[a,x+\frac{b}{4N}]\right)}. \tag{3}$$

For trait-decreasing alleles, the mean value of β does not depend on the derived allele frequency x, and is given by

$$\beta^-_{a,b} = \int_\gamma \Gamma[a,b,\gamma]\left(\frac{\gamma}{2N}\right)^\tau d\gamma = (2Nb)^{-\tau}\frac{\Gamma[a+\tau]}{\Gamma[a]}. \tag{4}$$

Combining terms and weighting by the frequency spectra for trait-increasing and trait-decreasing

alleles, we find that the mean value of β as a function of DAF x ($\bar{\beta}(x)$) is given by

$$\beta_{a,b}(x) = \frac{(8b)^{-\tau} N^{-2\tau} \Gamma[a+\tau] \left(-(4N)^{a+\tau}(x-1) + b^{a+\tau}(-\zeta[a+\tau, \frac{b}{4N}] + \zeta[a+\tau, 1-x+\frac{b}{4N}])\right)}{\Gamma[a] \left(-(4N)^{a}(x-1) + b^{a}(-\zeta[a, \frac{b}{4N}] + \zeta[a, 1-x+\frac{b}{4N}])\right)}. \quad (5)$$

We performed stochastic simulations under this model, in addition to our calculations. For the simulations, we used a weak distribution of selective effects ($\mathbb{E}[2Ns] \approx 8$) given by $\Gamma[a = 0.0415, b = 0.00515625]$, which was inferred from human conserved non-coding polymorphism data (Torgerson et al., 2009). Our results show that trait-increasing alleles will be more likely to increase in frequency (Fig. S1B), and will outnumber trait-decreasing alleles at all frequencies, resulting in $\beta_{a,b}(x) > 0$ at all frequencies (Fig. S1C). This implies that under this simple polygenic adaptation model, the S_β will increase monotonically in the direction of the selection (*i.e.*, if selection favors increases in trait values, $S_\beta(0, x)$ will be positive and monotonically increasing in x, while $S_\beta(0, x)$ will be negative and monotonically decreasing in x if lower trait values are preferred). Our analytical calculations from eqn. 5 (Fig. S1C, black curve) are in tight agreement with the simulations (Fig. S1C, points). Equations in this section were solved using *Mathematica*.

Mutational bias and negative selection

Negative selection against trait-altering alleles will also generate an increasing or decreasing βDAF relationship, if trait-increasing and trait-decreasing mutations are not equally likely to occur (Fig. S1E). To better understand this relationship quantitatively, we used analytical calculations under Eyre-Walker's quantitative trait model to calculate the relationship between β and DAF.

We define mutational bias δ as the proportion of new mutations that are trait-increasing, and as in the previous section, we suppose that effect sizes are given by $\beta = |s|^\tau$. In contrast to the previous section (but in accordance with the original Eyre-Walker model), we suppose that all causal alleles are deleterious, regardless of their direction of effect. We suppose that s is drawn from a Γ-distribution.

Under this model, we are able to calculate $\beta_{a,b}(x)$ using the same procedure as in the previous section. We find

$$\beta_{a,b}(x) = (1-2\delta) \frac{4N^{-\tau} \Gamma[a+\tau] \left(-\zeta[a+\tau, 1+\frac{b}{4N}] + \zeta[a+\tau, x+\frac{b}{4N}]\right)}{\Gamma[a] \left(-\zeta[a, 1+\frac{b}{4N}] + \zeta[a, x+\frac{b}{4N}]\right)}. \quad (6)$$

We performed stochastic simulations under this model for a variety of values of δ, again using a weak distribution of selection coefficients that was fit to human conserved non-coding sequences (Torgerson et al., 2009). We find excellent agreement between our simulations and the analytical predictions. When $\delta = 0.5$, trait-increasing and trait-decreasing alleles are exactly balanced, and there is no dependency of β on DAF. In contrast, as δ becomes increasingly biased, trait-decreasing alleles further outnumber trait-increasing alleles. Since larger effect alleles are subject to stronger selection, the difference is greater at low frequency than high frequency, generating a correlation between β and DAF. Taking $S_\beta(0, x)$ as the sum over the terms in eqn. 6, we find that S_β increases monotonically in magnitude in the same direction as the mutation bias under this model. In contrast to the mutational-bias only model, $S_\beta(0, x)$ does not increase linearly in magnitude as a function of x when selection acts.

Mutational bias and stabilizing selection with shifts

The previous sections show that a βDAF plot and S_β can capture signals of positive and negative selection as well mutational bias, but there is now substantial evidence that both positive and negative selection may act on complex traits. Indeed, it seems unlikely that polygenic adaptation will continue indefinitely

over long evolutionary times, because this would imply that the trait would continue to increase or decrease over very long timescales. A more natural way to model negative selection punctuated with periods of adaptation is through stabilizing selection with shifts in the fittest value of the phenotype (Jain and Stephan, 2017).

We develop a polygenic selection quantitative trait model that maps selection coefficients s to effect sizes β using the well-established Gaussian stabilizing selection model (Robertson, 1956; Barton, 1986). We suppose that stabilizing selection acts on a trait, and that the fittest value of the trait is ϕ_o (also referred to as the "trait optimum"), such that the fitness f of an individual with trait value ϕ is given by

$$f(\phi) = e^{\frac{-(\phi-\phi_o)^2}{w^2}}, \tag{7}$$

where w is the breadth of the fitness function. We additionally suppose that the trait ϕ has a normal distribution such that

$$P(\phi) = \frac{1}{\sqrt{2\pi\sigma^2}} e^{\frac{-(\phi-\bar{\phi})^2}{\sigma^2}}, \tag{8}$$

where σ is the standard deviation of the fitness distribution and $\bar{\phi}$ is the mean trait value in the population. Under these conditions, it is possible to solve for the per-generation, per-individual selection coefficient s as a function of the above model parameters for causal alleles of effect size β. We calculate s by marginalizing the fitness effect of a new mutation of effect size β across all fitness backgrounds. Our calculation proceeds similarly to previous work (Barton, 1986; Simons et al., 2018), although we retain the dependence on the current mean phenotype value ($\bar{\phi}$) and the phenotype optimum (ϕ_o), rather than assuming that the phenotype distribution is centered at the optimum. While the full expression for the expected change in allele frequency is provided in the next section, we note that when the trait is at equilibrium such that $\bar{\phi} = \phi_o$,

$$s \approx -\frac{\beta^2}{2\left(\sigma^2 + w^2\right)}, \tag{9}$$

and the expected frequency change δp for an allele at frequency p with effect size β when $\bar{\phi} = \phi_o$ is

$$\mathbb{E}[\delta p] \approx -\frac{\beta^2}{2\left(\sigma^2 + w^2\right)} p(1-p)(-1+2p), \tag{10}$$

which implies that the trait evolves as if underdominant when the mean population trait value is centered close to the optimum.

Recasting the selection coefficient in terms of the trait distribution

To calculate the time-dependent selection coefficient $s(t)$ of a site with effect size β, we first develop some results that allow us to recast the selection coefficient s at equilibrium as a function of the proportion of the population in which an allele of effect size β is fitness-increasing. Since the trait is normally distributed, the probability that an individual has phenotype value ϕ, $P(\phi)$, is given by $P(\phi) = \frac{1}{\sqrt{2\pi\sigma^2}} e^{\frac{-(\phi-\bar{\phi})^2}{\sigma^2}}$. To calculate the selection coefficient for an allele with effect size β, we then marginalize across all trait backgrounds and possible genotypes in the population to obtain the mean fitness effect, since the fitness effect varies across trait backgrounds according to $f(\phi)$. The three possible genotypes for a causal variable allele are denoted as aa (homozygous ancestral), ad (heterozygous), and dd (homozygous derived). For each genotype, we calculate the fitness w of an allele at frequency p as

$$w_{aa} = \int_{-\infty}^{\infty} f(\phi) P(\phi + 2p\beta) d\phi, \tag{11}$$

$$w_{ad} = \int_{-\infty}^{\infty} f(\phi + \beta) P(\phi + 2p\beta) d\phi, \tag{12}$$

$$w_{dd} = \int_{-\infty}^{\infty} f(\phi + 2\beta) P(\phi + 2p\beta) d\phi. \tag{13}$$

substituting in $P(\phi)$ and $f(\phi)$, these integrals can be solved to obtain $w_{aa} \propto e^{\frac{-(2p\beta+\phi_o-\bar{\phi})^2}{2(w^2+\sigma^2)}}$, $w_{ad} \propto e^{\frac{-((-1+2p)\beta+\phi_o-\bar{\phi})^2}{2(w^2+\sigma^2)}}$, and $w_{dd} \propto e^{\frac{-(2(-1+p)\beta+\phi_o-\bar{\phi})^2}{2(w^2+\sigma^2)}}$. We then can solve for the expected change in frequency $\mathbb{E}[\delta p]$ at time of an allele at frequency p as

$$\mathbb{E}[\delta p] = \frac{p(1-p)w_{ad} + p^2 w_{dd}}{2p(1-p)w_{ad} + p^2 w_{dd} + (1-p)^2 w_{aa}} - p, \tag{14}$$

Taking a series expansion about $\beta = 0$, we find that

$$\mathbb{E}[\delta p] \approx \frac{\beta\left(\phi_o - \bar{\phi}\right) p\,(1-p)}{w^2+\sigma^2} - \frac{\beta^2\left(p(1-p)(2p-1)\left(w^2+\sigma^2-\left(\bar{\phi}-\phi_o\right)^2\right)\right)}{2(w^2+\sigma^2)^2} \tag{15}$$

When $\bar{\phi} = \phi_o$, alleles evolve as if underdominant because $\mathbb{E}[\delta p] \approx -\frac{\beta^2}{2(\sigma^2+w^2)} p(1-p)(-1+2p)$. When $\bar{\phi} \neq \phi_o$, alleles may either be expected to increase in fitness (*i.e.*, be transiently positively selected) or decrease in frequency, depending on their effect size and the current mean population trait value $\bar{\phi}$. In our Wright-Fisher simulations, we replace the expected frequency change with eqn. 15 and track the current mean population trait value as a time-dependent quantity (see next section for more details).

Validation of simulations

We developed a custom simulator of our model in Python. Our simulator accommodates changes in population size, including explosive growth and bottlenecks, as well as any arbitrary distribution of selection coefficients. We perform a burn-in period of $5N$ generations for a simulated population of size N, during which we suppose that the population is close to equilibrium and hence s does not vary each generation. After the first burn-in, we perform an additional $5N$ generations of burn-in during which we recalculate $\mathbb{E}[\delta p]$ as a function of β, $\bar{\phi}$, and ϕ_o in each generation with eqn. 15. To calculate the current value of $\bar{\phi}$, we sum over all j causal alleles, such that $\bar{\phi} = \sum_j 2q_j\beta_j$, where q_j is the frequency of a site with effect size β_j.

For simulations of polygenic adaptation, at some time t_s during the simulations, we reset ϕ_o to a new value, which induces the trait distribution to be out-of-equilibrium with respect to the fitness function. During the out-of-equilibrium period, a portion of the causal sites will be positively selected (specifically those that are fitness increasing when marginalizing across all trait backgrounds, as described in the previous section), while the remaining sites will be fitness-decreasing. Each generation, we recalculate δp based on the current configuration of $\bar{\phi}$ and ϕ_o.

To validate our simulator, we simulated a complex selection and demographic model using previously published models of European demographic history (Gravel et al., 2011) and selection on human conserved elements (Torgerson et al., 2009) in SFS_CODE (Hernandez, 2008) and compared the SFS_CODE frequency spectrum to the frequency spectrum in our simulations. When no shift in the trait optimum occurs, selection coefficients in our model have the same expected value as in the standard Wright-Fisher model with underdominance, so the frequency spectra should be similar. However, since underdominance is not straightforward to simulate in SFS_CODE, for this set of validation simulations we replaced the underdominance term in our simulations with the standard genic selection model. Results of these simulations are plotted in Fig. S4. We observe good agreement between the two spectra overall, although our model results

in a slight over-representation of rare alleles and a slight under-representation of common alleles relative to SFS_CODE. Note that there is weak LD in the SFS_CODE simulations and that our selection model differs slightly, so we do not expect perfect agreement. For the SFS_CODE simulations, we used the following command line: `sfs_code 1 500 -N 1000 -n 100 -A -t 0.001 -r 0.0 -TE 0.405479 -Td 0 P 0 1.982738 -Td 0.265753 P 0 0.128575 -Td 0.342466 P 0 0.554541 -Tg 0.342466 P 0 55.48 -L 100 150 -l g 0.5 R -a N R -W 2 0 1 1 0.0415 0.00515625 -s <random_seed> -o <out>`

For the simulations presented in Fig. 1, the curves represent the mean over 100 independent simulations. We used $N = 7,000$ (where N is the ancestral population size) for the simulations in Fig. 1., but rescaled the population size for computational efficiency to 2,000 for parameter inference (see next section). The simulation code was implemented in Python and numpy, and will be freely available and posted on Github.

S_β in simulation

We performed simulations of Gaussian stabilizing selection with shifts in the optimal phenotype value for a wide range of parameter combinations. Since we ultimately apply our results to data from European GWAS, we apply a European demographic model (including ancestral expansion and bottleneck events, as well as recent exponential growth) that was fit to patterns of genomic diversity (Gravel et al., 2011). Our goal in these simulations is to understand the qualitative behavior of S_β as a function of evolutionary parameters (Fig. 1C-E), and in subsequent sections we develop a more quantitative approach for mapping evolutionary parameters to observed patterns in GWAS summary statistics.

For simulations shown in Fig. 1, we used $N = 7,000$ (in accordance with (Gravel et al., 2011)), a mutational bias of $\delta = 0.4$, $h^2 = 0.8$, and selection strength $\omega = 1$. Effect sizes drawn from a Gamma distribution with $a = 0.037$ and $b = 0.0008$, and assumed a genome-wide polygenicity of 0.02 (*i.e.*, 2% of target sites have a non-zero effect on phenotype). While these choices are arbitrary, we use rejection sampling to find parameter combinations that fit the observed data in the subsequent section.

Inferring evolutionary parameters

We developed a rejection-sampling based approach to infer evolutionary parameters (Tavaré et al., 1997). Rejection sampling uses informative summary statistics in model-based simulations to infer an approximate posterior distribution of model parameters. Simulations are performed under the model with parameters drawn from a wide range of possible combinations, and then the subset of simulations that most closely match the observed data are retained to build the posterior. The remaining simulations are rejected.

We performed simulations of Gaussian stabilizing selection with shifts in the optimal phenotype value using parameter values that were sampled from broad prior distributions, and we fit these simulated data to the observed $S_\beta(0.01, x)$ data for our phenotypes (we exclude alleles below 1% frequency to avoid the potential effects of rare variant stratification). As summary statistics, we take $S_\beta(0.01, x)$ for $x \in \{0.02, 0.03, 0.04, 0.07, 0.12, 0.22, 0.52, 0.62, 0.72, 0.82, 0.92\}$. Additionally, since the absolute magnitude of S_β depends on the units of the effect sizes, we defined scaled $S_\beta(x_i, x_f)$ as $\frac{S_\beta(x_i,x_f)}{S_\beta(0.01,0.99)}$, and use the scaled summary statistics as input to our method. As a final summary statistic, we take $\frac{S_\beta(0.01,0.99)}{k\bar{\beta}}$, where $\bar{\beta}$ is the mean effect size over all effect sizes in the study (or simulation) and k is the number of frequency bins ($k = 100$ here). As we showed earlier in the Supplemental Information, S_β has expectation $k\bar{\beta}$ when only mutational bias acts on the trait, so this summary statistic has expectation 1 when only mutational bias acts on the trait.

We performed 10^5 simulations, drawing evolutionary parameters from very wide prior distributions. Parameters of the model included heritability (h^2, uniform from 0.5 to 1), shift in optimum phenotype ($\Delta\phi$, uniform on -5 to 5 in units of the standard deviation of the ancestral trait distribution), polygenicity

(Ψ, chosen uniformly from 0.004 to 0.02 of sites genome-wide being causal), effect size distribution parameters (chosen from the square root of a Γ-distributed according to a and b, with a chosen to be within a factor of 4 greater or less than 0.04 and b chosen to be within a factor of 4 of 8e-5 – this enforces selection coefficients to be drawn from a Γ-distribution), mutational bias δ (uniform on 0.25 to 0.75), the time of the shift in optimal phenotype (t_s, uniform from -1 to 0.4 in coalescent units, corresponding to the time period ranging from 500,000 to 17,500 years ago), and ancestral uncertainty (unifom from 0.7 to 1, where 1 represents perfect ancestral assignment). Because we vary both heritability and the effect size distribution, we did not additionally vary the selection parameter of Gaussian stabilizing selection ω, which we set at 1. We rescaled the population size to $N = 2 \times 10^3$ for computational efficiency (the ancestral population size in the demographic model is $N = 7 \times 10^3$). Although we do not directly vary the selection coefficient distribution (because selection coefficients depend on effect sizes and the current trait variance σ^2, and we sample effect size parameters as opposed to selection parameters), our simulations include both very weak selection per site and strong selection per site. After each simulation finishes, we mix the causal alleles with neutral alleles that are simulated under the same demographic model, and have effect size 0, representing the portion of the genome that is not causal for the trait but is included in the GWAS. We calculate the sum of squared differences between our simulated and observed statistics for all 10^5 simulations, and retain the 0.25% of simulations that minimize this statistic.

To test our rejection sampling method, we masked the input parameter set of each simulation and attempted to infer the parameter values that were used to run the simulation. We used the maximum *a posteriori* estimate as a point estimate of the parameter value for these experiments. We found high predictability of the direction of both mutational bias δ and $\Delta\phi$ (Fig. 3C&D), and noisy estimation of the magnitude of these parameters. Most other parameters were poorly predicted. We found that the true timing of selection events was highly correlated with the inferred timing, but a large number of outlier estimates make the estimates of this parameter less trustworthy, so we do not report it. All other parameters were inferred with low accuracy, hence we only report δ and $\Delta\phi$.

In addition to the power to detect mutation rate bias (δ) and shifts in optimal phenotype value ($\Delta\phi$), we also considered the false positive rate for detection of these parameters (Fig. S5). We examined the subset of simulations among our 10^5 that had $|\Delta\phi| < 0.25$ and the subset with $0.45 < \delta < 0.55$ and assessed the proportion of these simulations for which we estimated maximum *a posteriori* parameters larger than y for all estimated values y. We found that the false positive rate is high for both small mutation rate biases and weak shifts, but low for effects as large as those we infer in the data, implying that our method is unlikely to result in a multiple false positives for shifts and mutation rate biases. Note that this null is very conservative, because all of the simulations we used to assess false positive rate include stabilizing selection, and the δ false positive simulations include shifts in selection while the $\Delta\phi$ false positive simulations include bias in mutation rate.

It should be noted that while our empirical selection detection method incorporates linkage, our rejection sampling method does not. Linkage between causal alleles and non-causals could cause the data to have larger deviations from 0 in S_β than our simulations, possibly causing our estimates of the parameters to be upwardly biased. For this reason (and because the estimates of parameters are noisy in our simulations), we focus primarily on the direction of the effects rather than their magnitudes.

Empirical data analyses

Aggregating phenotype data

We obtained GWAS summary data from several published studies for nine different phenotypes as discussed in the main text (Wood et al., 2014; Shungin et al., 2015; Locke et al., 2015; CDG Psychiatric Genomics Consortium, 2013; Franke et al., 2010; Day et al., 2015; Global Lipids Genetics Consortium et al., 2013; Okbay et al., 2016). We obtained allele frequencies for each allele in each study from the

GWAS summary data in the corresponding study. To calculate S_β for each study, we first needed to polarize all the alleles by their derived/ancestral status. We obtained inferred derived/ancestral states for each allele from the 1000 Genomes project (Thousand Genomes Project Consortium et al., 2015). Our permutation method requires that each allele then be assigned to a LD block within the genome (Berisa and Pickrell, 2016). To assign each of these alleles to LD blocks, we also used the 1000 Genomes data to obtain the genomic coordinates for each allele. Alleles for which we could not assign states or LD blocks were excluded.

Calculating S_β and implementing PASTEL

To account for LD in selection tests for complex traits using GWAS summary data, we divided the genome into 1,703 LD blocks, which were previously identified as being approximately independent (Berisa and Pickrell, 2016). For each LD block, we then select a random sign (positive or negative with equal probability), and multiply all the effect sizes in the LD block by this sign. We then recompute summary statistics (such as the correlation between frequency and MAF) on the randomized data. By repeating this procedure, we generate a null distribution for the test statistic. This method maintains the correlations between effect sizes generated by LD, the site frequency spectrum of the sampled alleles, and the joint distribution of the absolute value of effect size and allele frequency, while breaking any relationship between effect sizes and allele frequency. Note that this is a conservative permutation, because many of the alleles within an LD block are not linked or only weakly linked. We further consider the robustness of our method to population stratification in a subsequent section, which is a persistent potential source of false positives for studies of selection. To assess significance, we perform a two-tailed test comparing the observed value of the test statistic to the permutation-based null distribution. We performed 2,000 permutations for each phenotype. We name this test PASTEL, or the Polygenic Ancestral Selection Test Encompassing Linkage.

We developed custom software implementing PASTEL in Python, which is freely available upon request and will be posted on Github. To calculate S_β, we group alleles into 1% frequency bins – without performing this grouping, many high frequency bins would have very few alleles and very noisy estimates of $\overline{\beta}$. We selected 1% because it strikes a balance between obtaining low standard errors on $\overline{\beta}$ and finely parsing the allele frequency space, but we note that other choices of bin size could potentially improve our power.

Replication data & analysis

As a replication cohort for our top three selection signals, we obtained GWAS summary statistics from the UK Biobank (UKBB) from https://data.broadinstitute.org/alkesgroup/UKBB/ (height, BMI, and educational attainment – note that approximately 1/4 of the UKBB samples were included in Okbay *et al*, so the studies are not completely independent). We used the PASTEL framework to calculate S_β on each phenotype, and estimate the linkage-adjusted variance in the test-statistic. We perform a one-tailed test for significance, since we have an expectation for the sign of S_β from our first set of findings. We replicate our findings for both BMI ($p = 0.0095$) and educational attainment ($p < 5e-4$) (Fig. S18). Perhaps surprisingly, height did not replicate (see main text for discussion of possible explanations).

In addition to S_β, we performed a replication study at signals of selection that were used in previous projects to identify signals of selection on height in the GIANT study. One study identified a positive correlation between effect size and allele frequency (Yang et al., 2015), while another found a correlation of allele frequency difference between northern and southern Europe and the p-value rank of the height increasing-allele (Turchin et al., 2012). Neither of these correlations were replicated in the UK Biobank summary statistics (Fig. S6).

Neanderthal alleles

A list of Neanderthal alleles that were inferred with the S^* statistic (Plagnol and Wall, 2006) was generously provided by Rajiv McCoy and Josh Akey. In analyses using Neanderthal alleles, we masked all alleles that were not present in this dataset. The dataset includes 139,694 SNPs, 139,381 of which we were able to map to rs numbers and use in our analysis.

The impact of ancestral uncertainty on S_β

Ancestral states are not directly observed in genomic data, and are typically inferred by comparing human sequences to those of an out-group. The underlying assumption is that the allelic state in the out-group represents the most likely ancestral state for the allele. While this approach correctly assigns the ancestral state for the majority of alleles, it does not account for recurrent fixation events at a single site, leading to some rate of ancestral misassignment. Since our method to detect selection compares ancestral and derived alleles, we sought to understand how ancestral misassignment would impact our inferences.

Ancestral misassignment will tend to decrease the absolute value of S_β within each frequency bin, and hence decrease our power. To see this, suppose that for a given minor allele frequency x, we misassign ancestral state with probability $1-p$, and $\Psi(x)$ is the number of derived alleles observed at frequency x. We note that we can rewrite S_β as the difference in mean beta between ancestral and derived alleles of equal minor allele frequency (*i.e.*, $S_\beta = \sum_x \bar{\beta}_D(x) = \sum_x \frac{1}{2}\left(\bar{\beta}_D(x) - \bar{\beta}_A(x)\right)$. The expected value of the the test statistic within this bin is then

$$\mathbb{E}[S_\beta(x)] = \frac{1}{2}\left(\left(p\Psi(x)\overline{\beta}_D + (1-p)\Psi(1-x)\overline{\beta}_A\right) - \left(p\Psi(1-x)\overline{\beta}_A + (1-p)\Psi(x)\overline{\beta}_D\right)\right), \tag{16}$$

where β_D is the effect size of derived alleles and β_A is the effect size of ancestral alleles. Note that if $p = 0.5$, we are randomly guessing at ancestral states, and $\mathbb{E}[S_\beta(x)] = 0$. If $p < 0.5$, then the absolute value of $\mathbb{E}[S_\beta(x)]$ is strictly less than it's true value (*i.e.*, the value that would be observed with no ancestral uncertainty).

While this analysis shows that ancestral uncertainty serves to make our analyses more conservative, we also sought to understand its potential impact on the observed relationship between allele frequency and effect size (Fig. S8). Because $\Psi(x)$ is generally much larger than $\Psi(1-x)$ for $x < 0.5$ (*i.e.*, there are more rare alleles than common alleles in genomic sequencing data), we expect that the impact of ancestral uncertainty will be greatest at very high derived allele frequencies (*e.g.*, $x > 0.9$). We fit a linear model by regressing the mean effect size on allele frequency for the observed height data for derived alleles in the frequency range 40-60%, and extrapolated this curve out to 100% frequency, supposing that frequencies near 50% were only modestly impacted by ancestral uncertainty. We then simulated the impact of ancestral uncertainty at various levels from $p = 1\%$ to $p = 10\%$. At $p = 10\%$ uncertainty we see a striking resemblance between our simulated data and the observed data. We conclude that moderate levels of ancestral uncertainty are likely responsible for the "S" shaped curve that we observe for many of our phenotypes.

Supplemental Figures

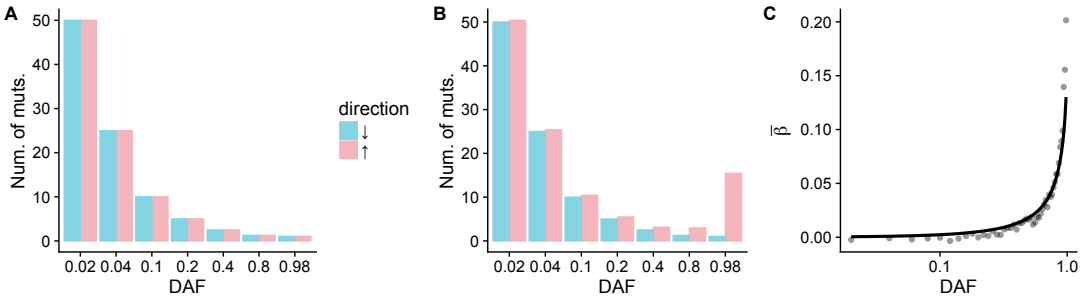

Figure S1: A: When selection does not prefer either trait-increasing or trait-decreasing alleles, and mutation bias does not act on a trait, then trait-increasing (pink) and -decreasing (blue) alleles are expected to have identical frequency spectra and equal mean β values within each frequency bin. B: When selection acts to increase a trait, trait-increasing alleles will increase in frequency and persist longer than trait-decreasing alleles, resulting in a relationship between $\bar{\beta}$ and frequency. C: $\bar{\beta}$ vs DAF for a toy model of where trait-increasing alleles are favored. The black line represents an analytical calculation (eqn. 5) while the black points are the results of stochastic simulations.

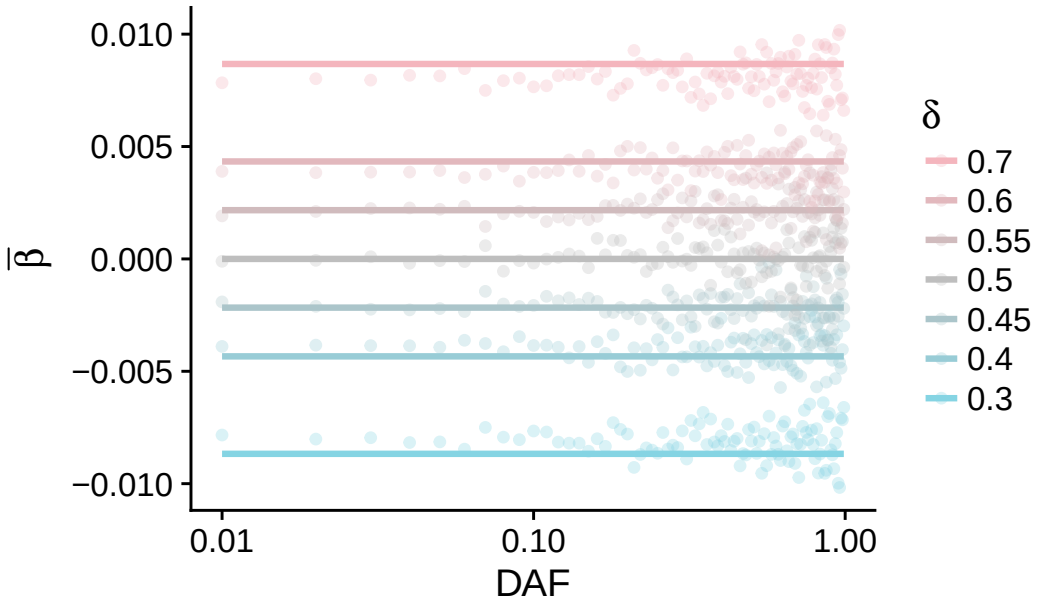

Figure S2: The relationship between β and DAF when only mutational bias acts on the trait (*i.e.*, there is no selection). Mean β is shifted in the direction of the bias, but does not depend on DAF.

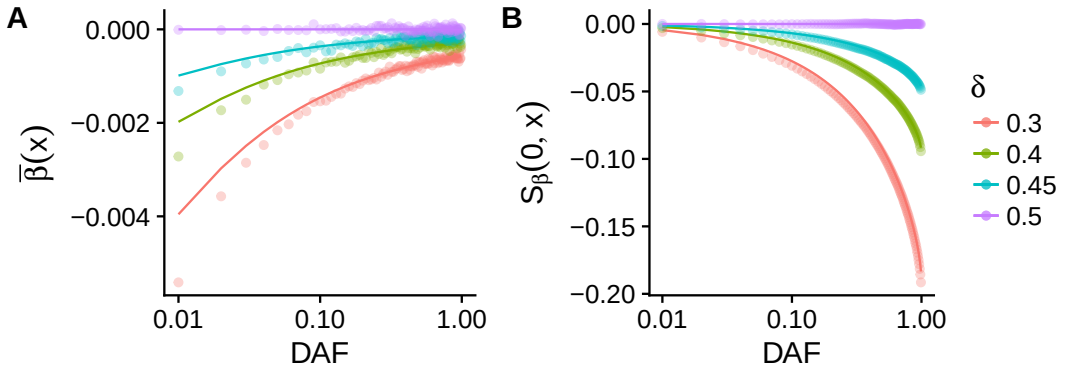

Figure S3: A: A βDAF plot for various values of mutational bias (δ) towards trait decreasing alleles for traits under selection. B: $S_\beta(0, x)$ for the same models in A. The solid lines represent the results of analytical calculations (eqn. 6) while the points represent stochastic simulations.

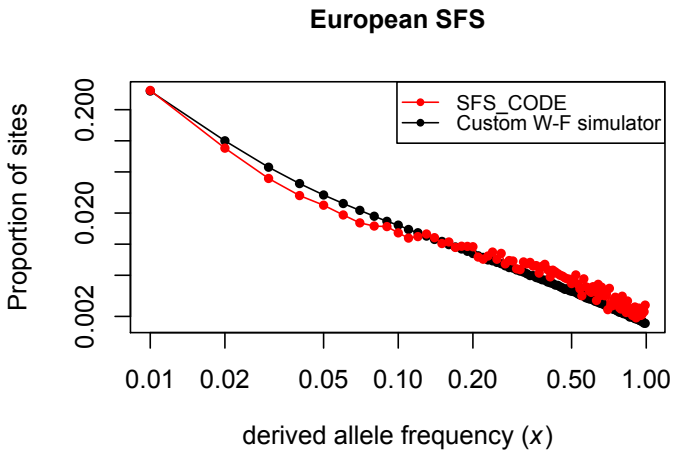

Figure S4: A comparison of simulated frequency spectra for a complex demographic/selection model for our Wright-Fisher simulator (black) and SFS_CODE (red).

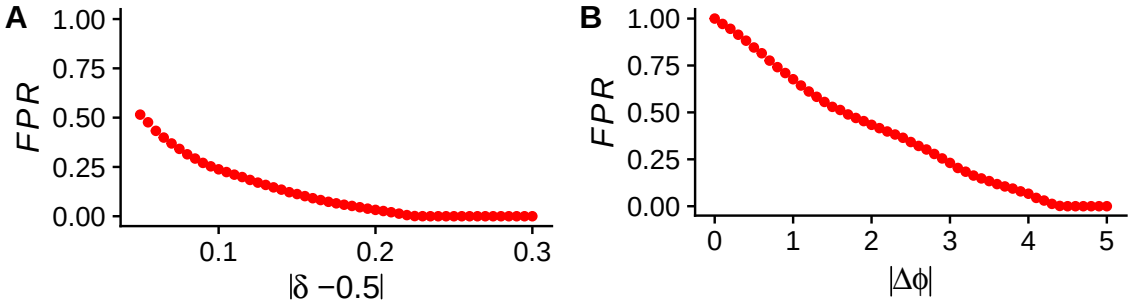

Figure S5: Conservative False Positive Rate estimation for detection of mutation rate bias and shifts in optimal phenotype value.

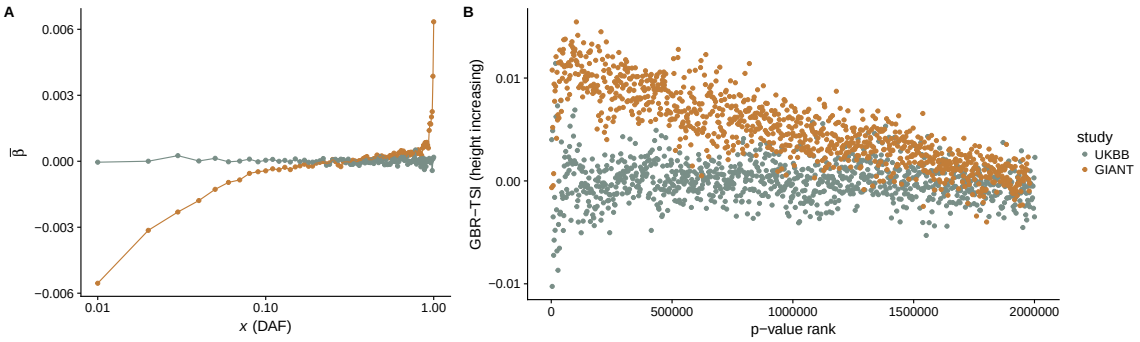

Figure S6: Correlation between mean effect size and allele frequency (A) and correlation the difference in frequency between northern and southern Europe for the height increasing allele and p-value rank (B) in the GIANT study (gold) and the UK Biobank (gray). Note that alleles were grouped in to bins of 2,000 by p-value and were not thinned by linkage.

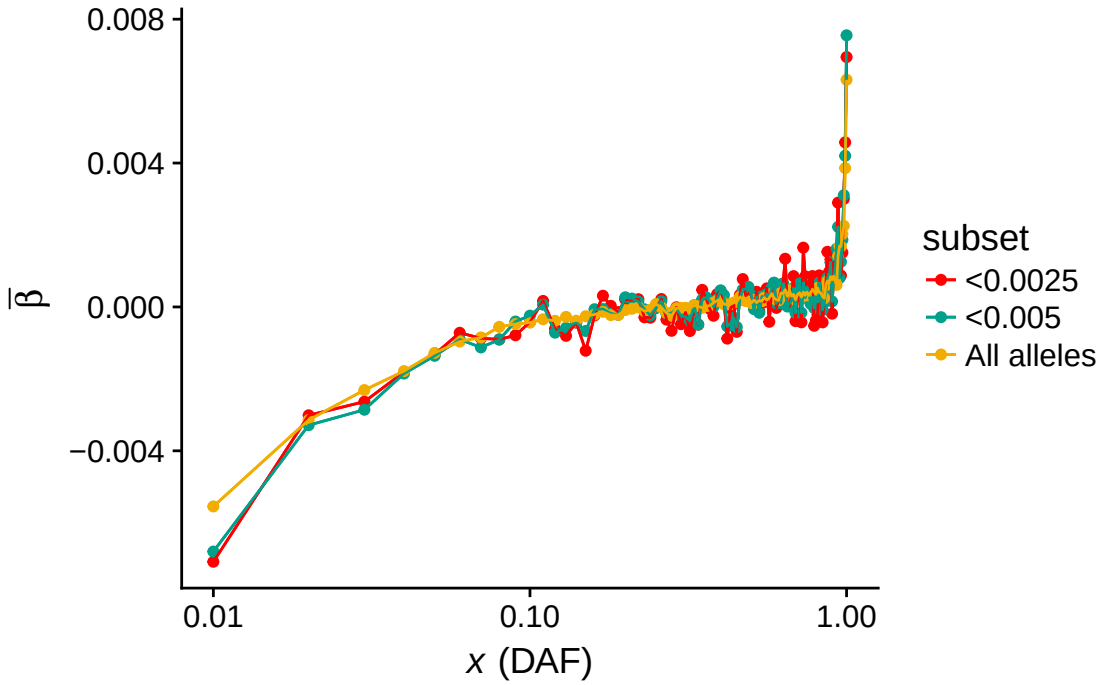

Figure S7: βDAF plot for alleles in GIANT as a function of the difference in derived allele frequency between northern (Great Britain; GBR) and southern (Tuscan Italians; TSI) Europe in the 1000 Genomes Project.

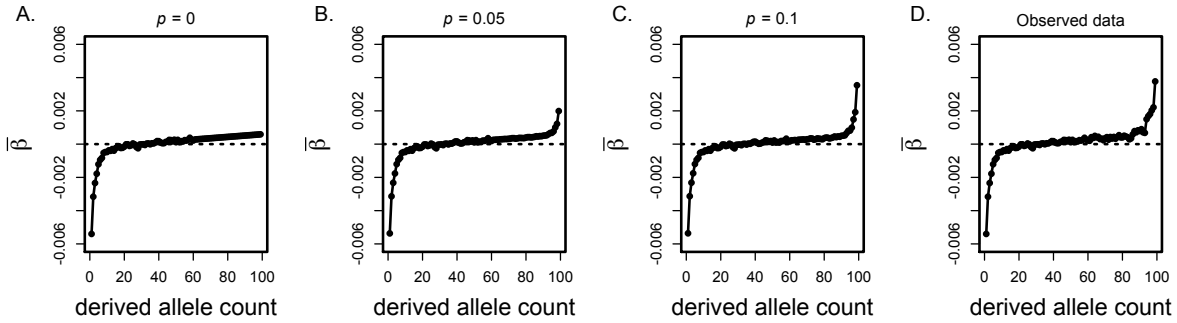

Figure S8: The impact of ancestral uncertainty on the observed value of mean β as a function of derived allele count x. Panel A shows results corresponding to no uncertainty ($p = 0$), in B $p = 0.05$, in C $p = 0.1$, and D shows the observed GIANT height data.

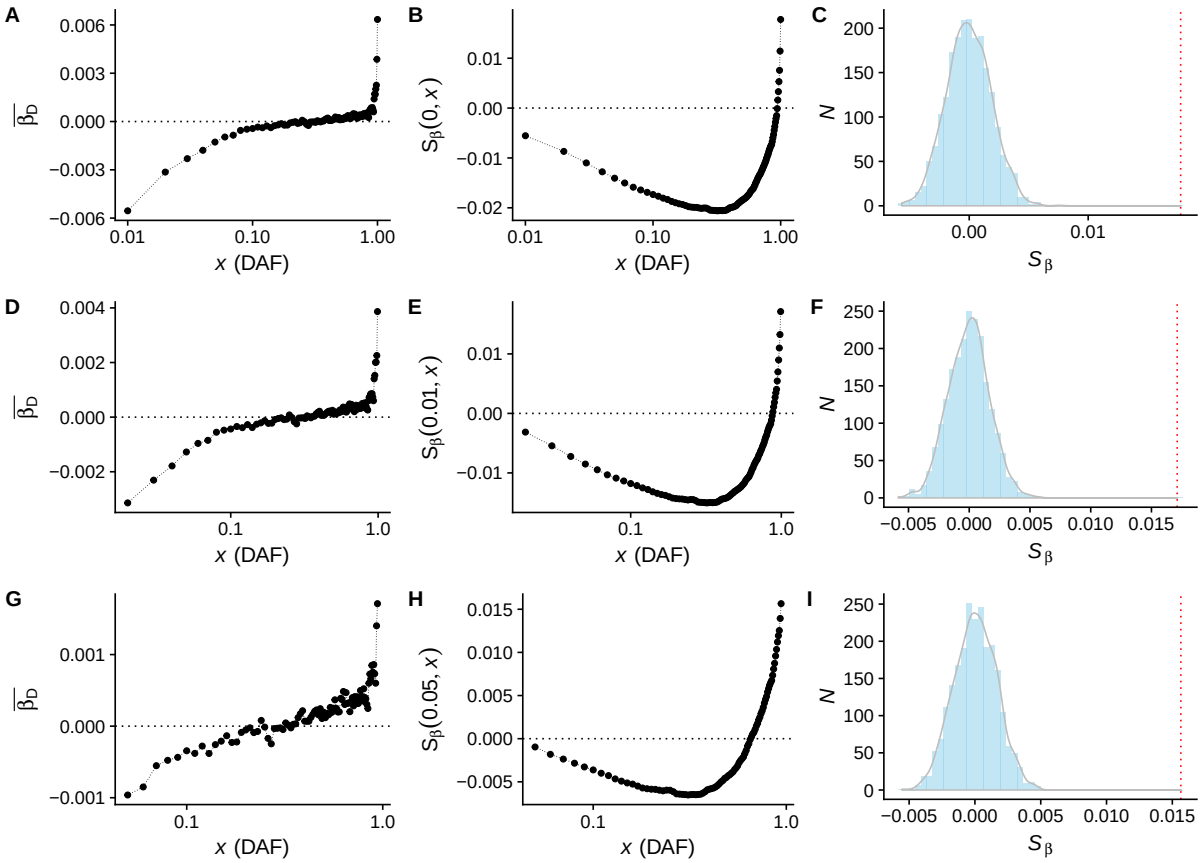

Figure S9: S_β for height. The panels in the left column show the relationship between allele frequency and $\overline{\beta}$, the middle column displays the cumulative value of $S_\beta(x_i, x_f)$, and the right columns show the null distribution of S_β given by our permutation test, PASTEL. Panels A-C correspond to $x_i = 0$ and $x_f = 1$, panels D-F correspond to $x_i = 0.01$ and $x_f = 0.99$, and panels G-I correspond to $x_i = 0.05$ and $x_f = 0.95$

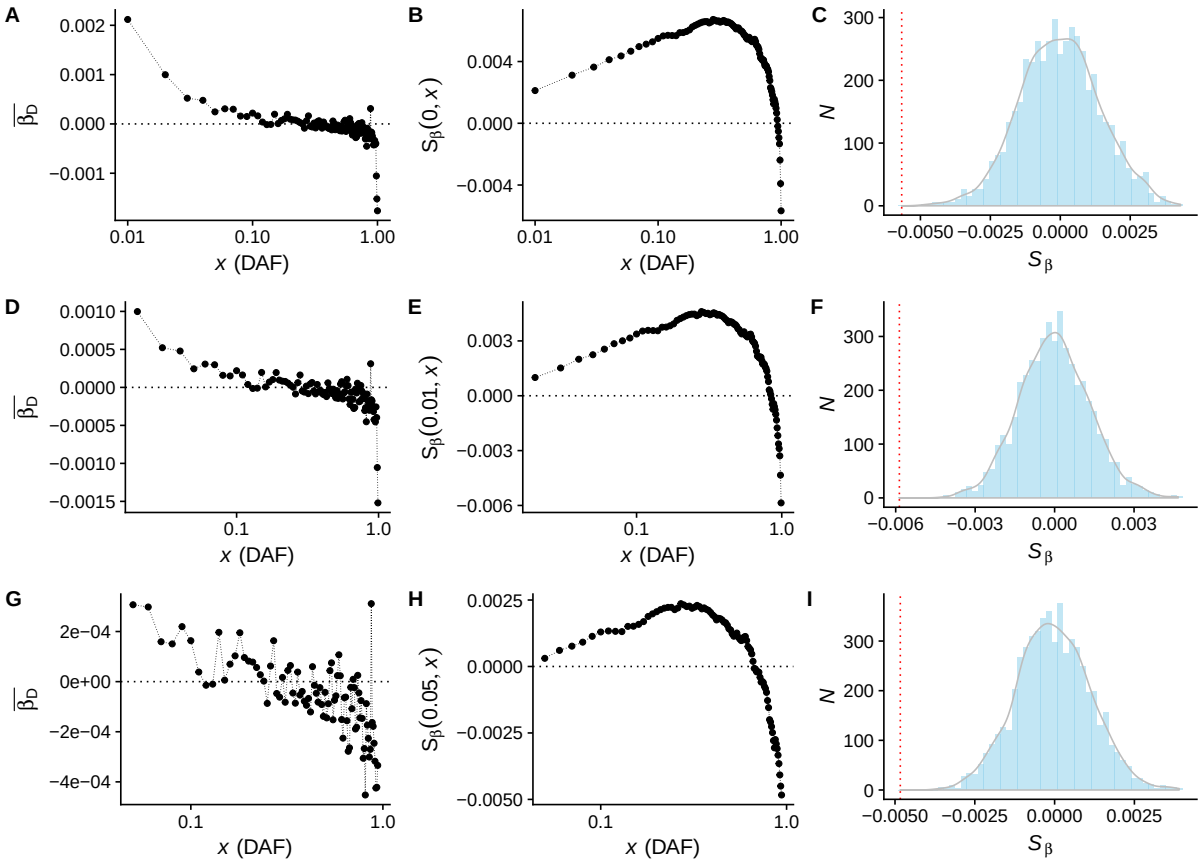

Figure S10: S_β for BMI. The panels in the left column show the relationship between allele frequency and $\overline{\beta}$, the middle column displays the cumulative value of $S_\beta(x_i, x_f)$, and the right columns show the null distribution of S_β given by our permutation test, PASTEL. Panels A-C correspond to $x_i = 0$ and $x_f = 1$, panels D-F correspond to $x_i = 0.01$ and $x_f = 0.99$, and panels G-I correspond to $x_i = 0.05$ and $x_f = 0.95$

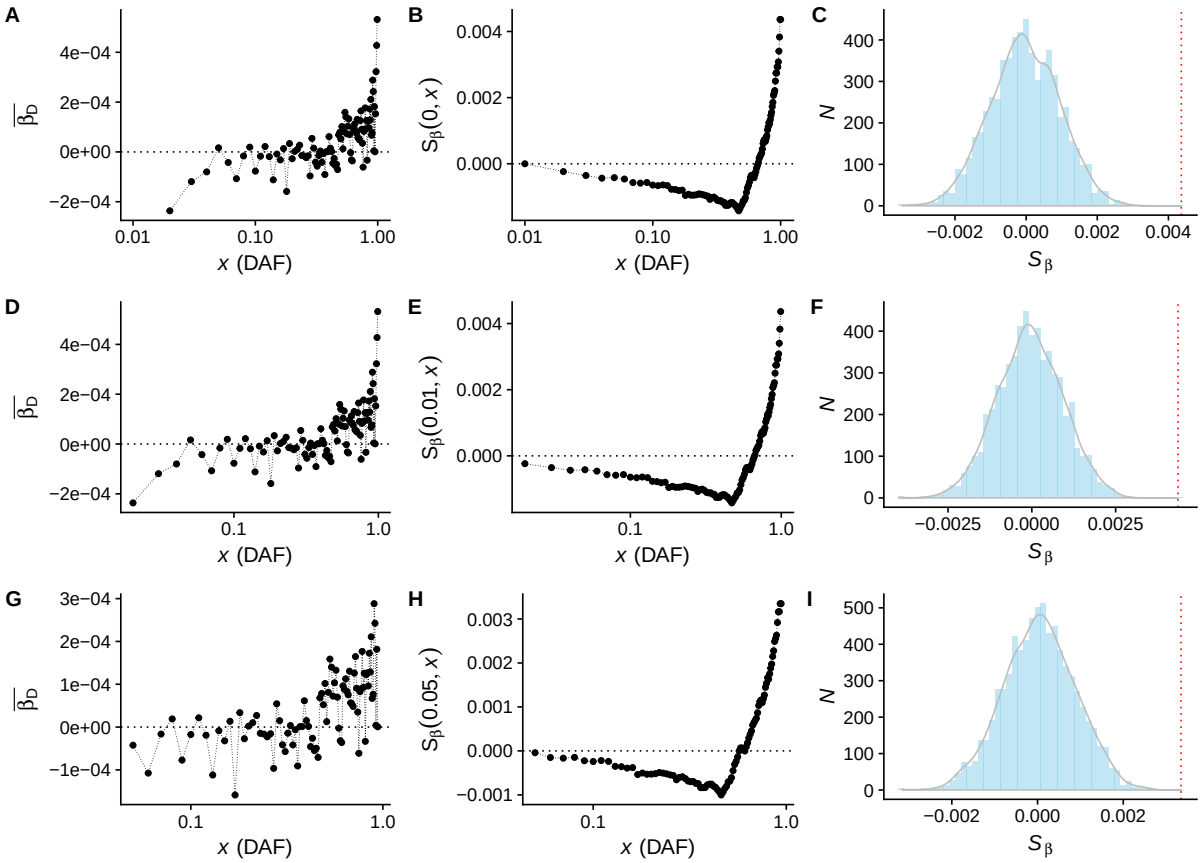

Figure S11: S_β for educational attainment. The panels in the left column show the relationship between allele frequency and $\overline{\beta}$, the middle column displays the cumulative value of $S_\beta(x_i, x_f)$, and the right columns show the null distribution of S_β given by our permutation test, PASTEL. Panels A-C correspond to $x_i = 0$ and $x_f = 1$, panels D-F correspond to $x_i = 0.01$ and $x_f = 0.99$, and panels G-I correspond to $x_i = 0.05$ and $x_f = 0.95$. Note that the results for A-C are the same as D-F because no alleles under 1% were included in the summary data for this study.

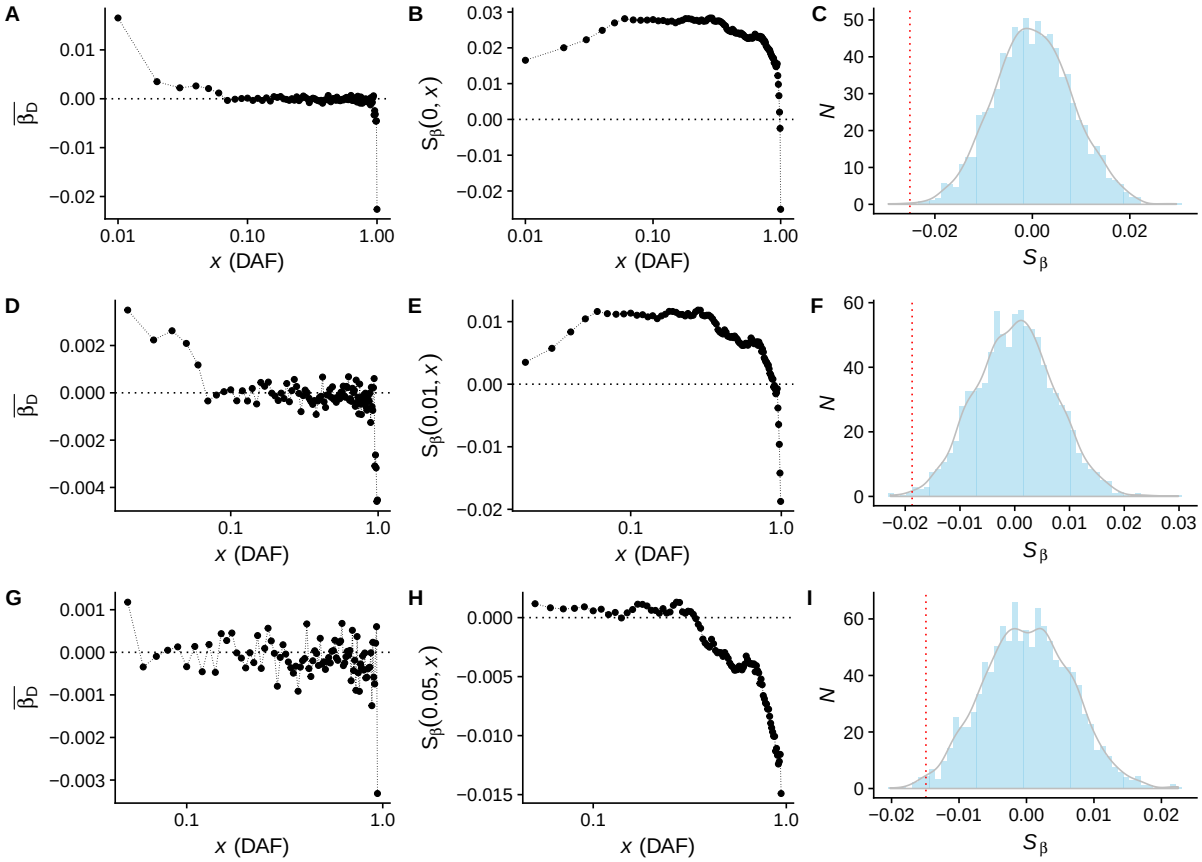

Figure S12: S_β for Crohn's disease. The panels in the left column show the relationship between allele frequency and $\overline{\beta}$, the middle column displays the cumulative value of $S_\beta(x_i, x_f)$, and the right columns show the null distribution of S_β given by our permutation test, PASTEL. Panels A-C correspond to $x_i = 0$ and $x_f = 1$, panels D-F correspond to $x_i = 0.01$ and $x_f = 0.99$, and panels G-I correspond to $x_i = 0.05$ and $x_f = 0.95$

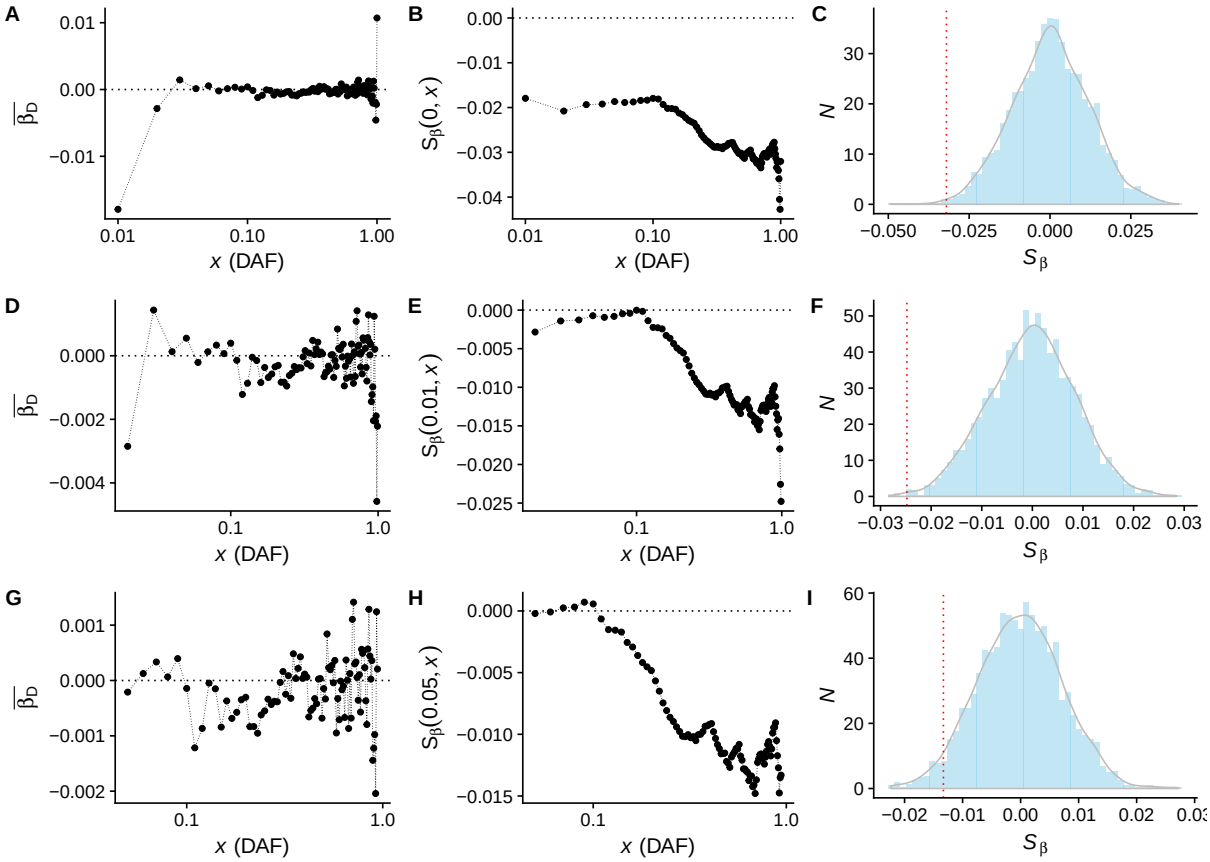

Figure S13: S_β for schizophrenia. The panels in the left column show the relationship between allele frequency and $\overline{\beta}$, the middle column displays the cumulative value of $S_\beta(x_i, x_f)$, and the right columns show the null distribution of S_β given by our permutation test, PASTEL. Panels A-C correspond to $x_i = 0$ and $x_f = 1$, panels D-F correspond to $x_i = 0.01$ and $x_f = 0.99$, and panels G-I correspond to $x_i = 0.05$ and $x_f = 0.95$

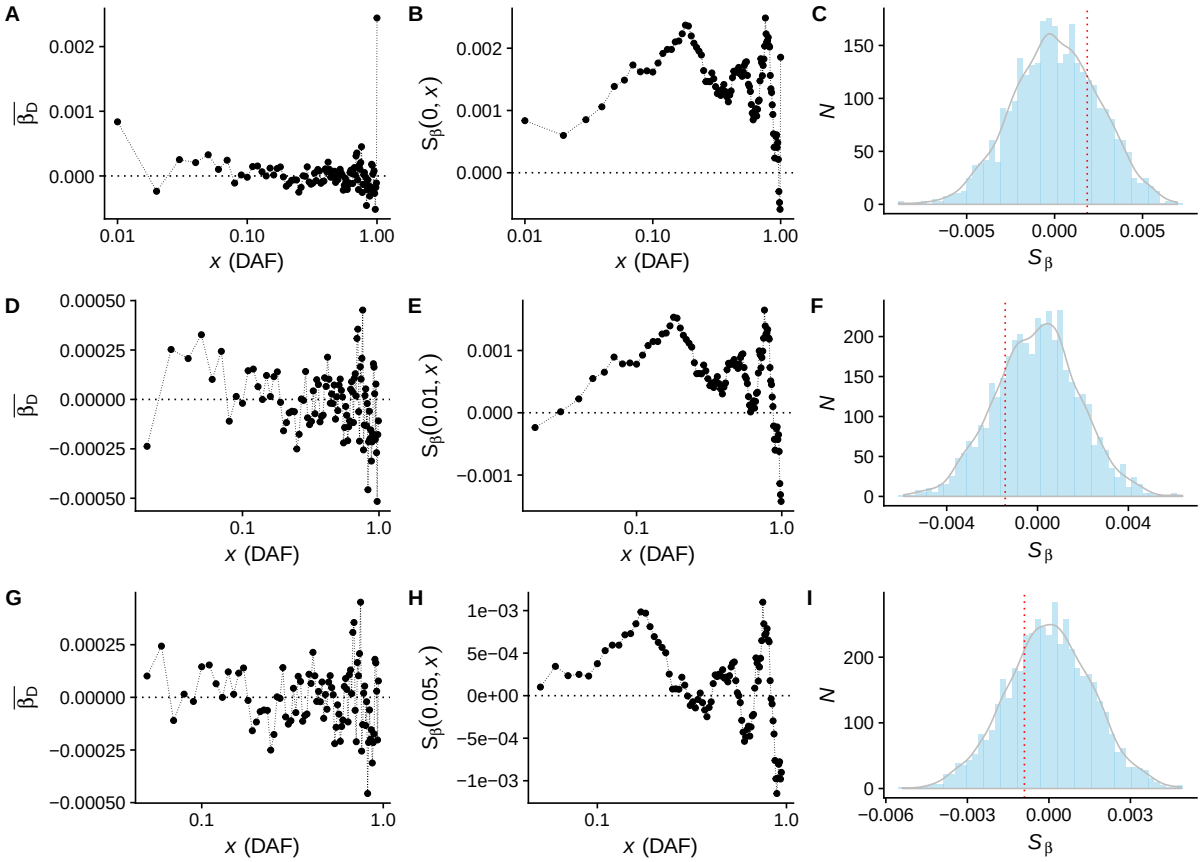

Figure S14: S_β for global lipid levels. The panels in the left column show the relationship between allele frequency and $\overline{\beta}$, the middle column displays the cumulative value of $S_\beta(x_i, x_f)$, and the right columns show the null distribution of S_β given by our permutation test, PASTEL. Panels A-C correspond to $x_i = 0$ and $x_f = 1$, panels D-F correspond to $x_i = 0.01$ and $x_f = 0.99$, and panels G-I correspond to $x_i = 0.05$ and $x_f = 0.95$

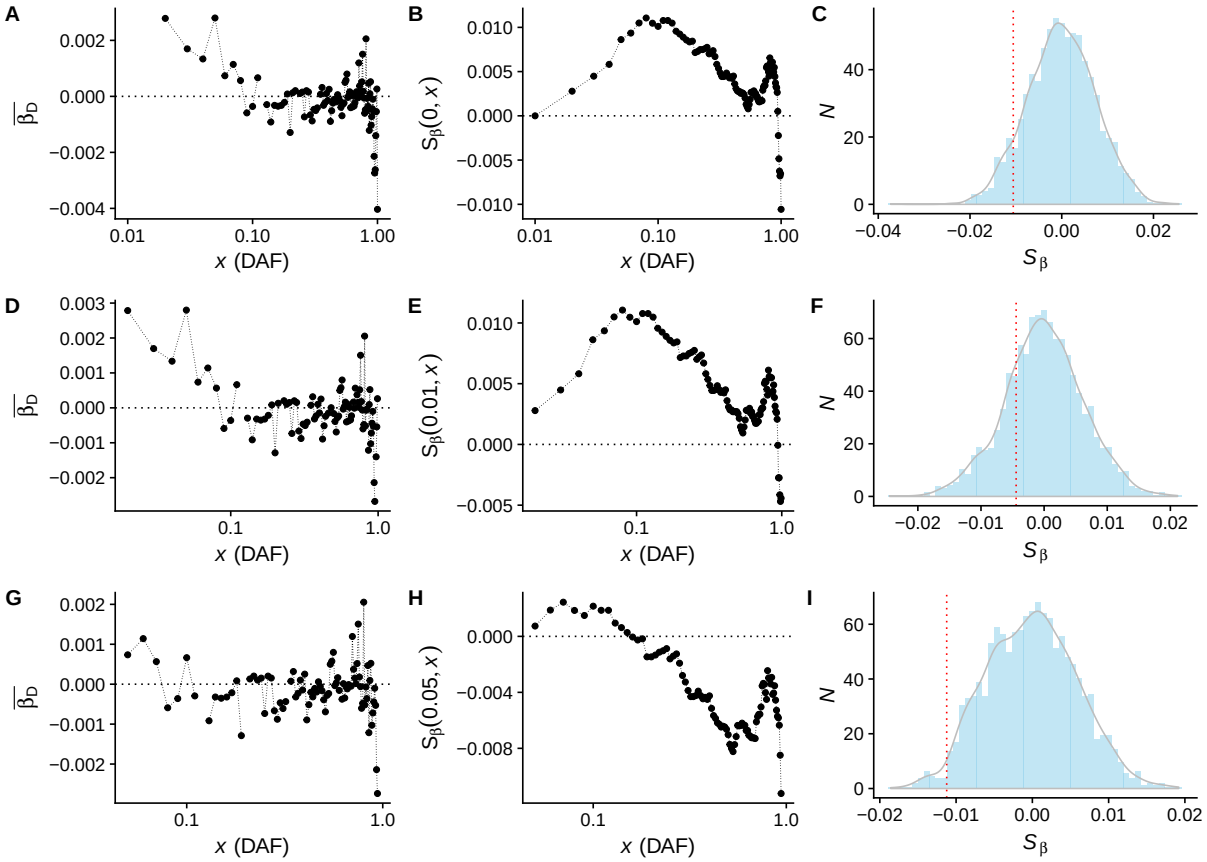

Figure S15: S_β for menopause onset. The panels in the left column show the relationship between allele frequency and $\overline{\beta}$, the middle column displays the cumulative value of $S_\beta(x_i, x_f)$, and the right columns show the null distribution of S_β given by our permutation test, PASTEL. Panels A-C correspond to $x_i = 0$ and $x_f = 1$, panels D-F correspond to $x_i = 0.01$ and $x_f = 0.99$, and panels G-I correspond to $x_i = 0.05$ and $x_f = 0.95$

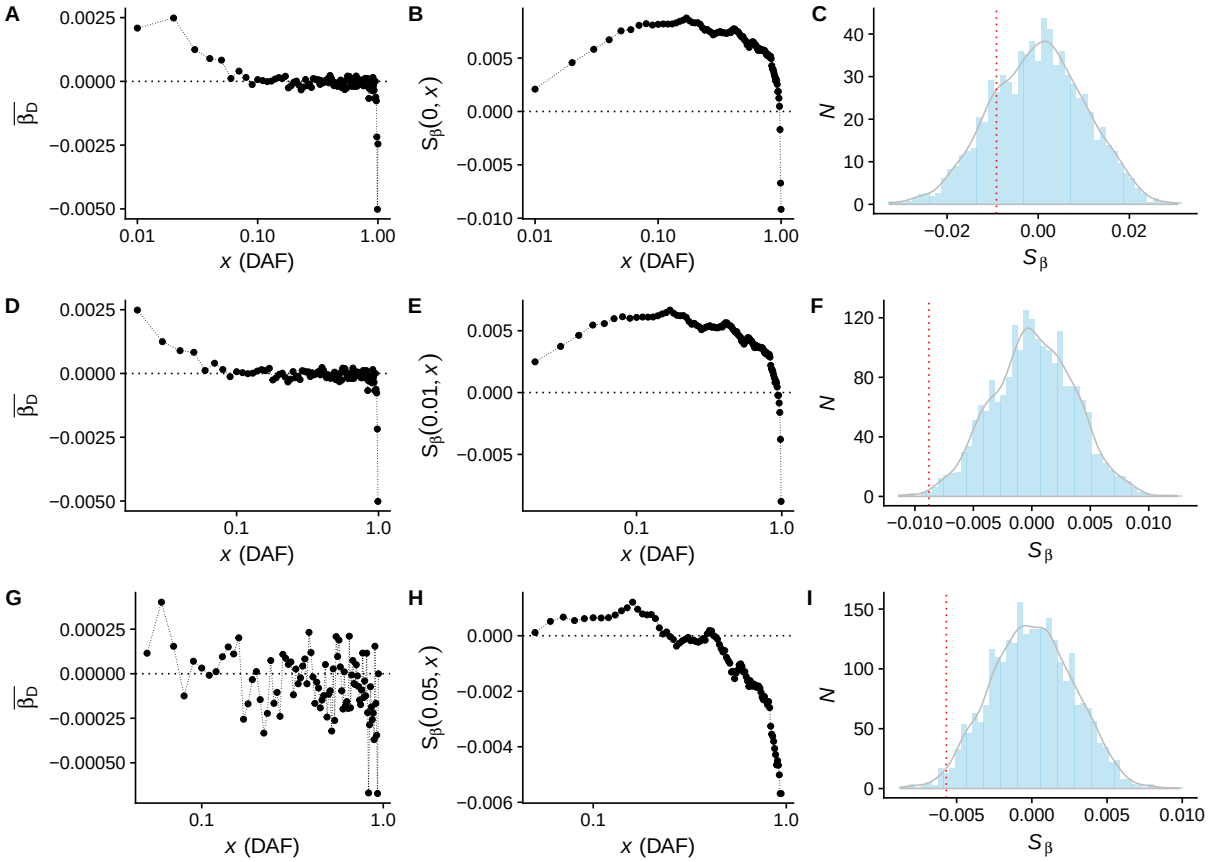

Figure S16: S_β for major depression. The panels in the left column show the relationship between allele frequency and $\overline{\beta}$, the middle column displays the cumulative value of $S_\beta(x_i, x_f)$, and the right columns show the null distribution of S_β given by our permutation test, PASTEL. Panels A-C correspond to $x_i = 0$ and $x_f = 1$, panels D-F correspond to $x_i = 0.01$ and $x_f = 0.99$, and panels G-I correspond to $x_i = 0.05$ and $x_f = 0.95$

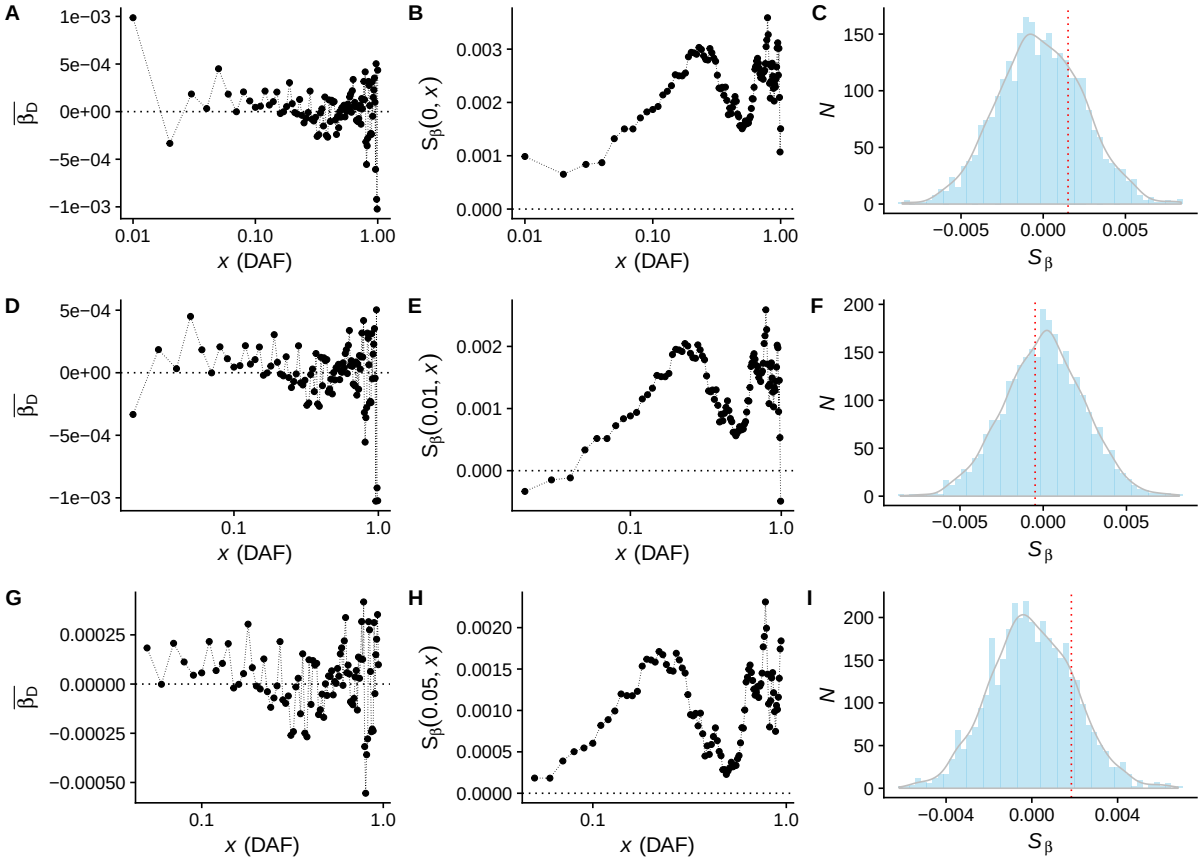

Figure S17: S_β for waist-hip ratio adjusted for BMI. The panels in the left column show the relationship between allele frequency and $\overline{\beta}$, the middle column displays the cumulative value of $S_\beta(x_i, x_f)$, and the right columns show the null distribution of S_β given by our permutation framework, PASTEL. Panels A-C correspond to $x_i = 0$ and $x_f = 1$, panels D-F correspond to $x_i = 0.01$ and $x_f = 0.99$, and panels G-I correspond to $x_i = 0.05$ and $x_f = 0.95$

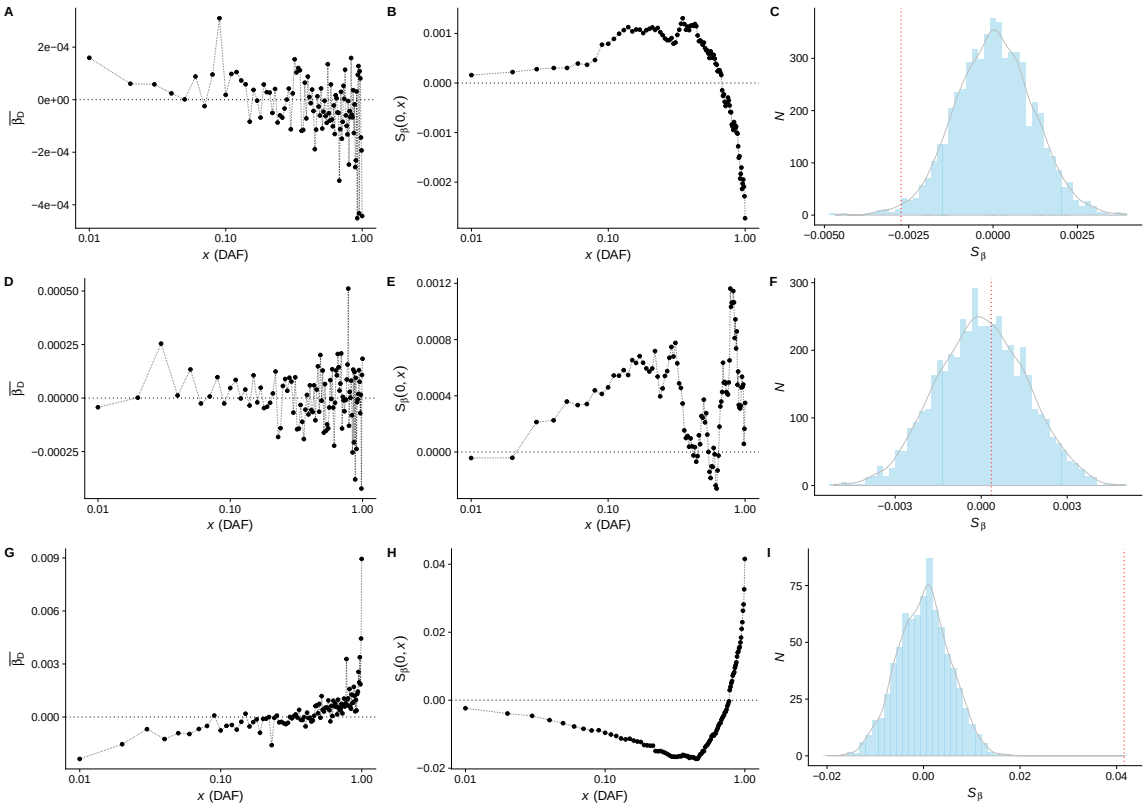

Figure S18: S_β for BMI (A-C), height (D-F), and educational attainment (G-I) in the UK Biobank. The panels in the left column show the relationship between allele frequency and $\overline{\beta}$, the middle column displays the cumulative value of $S_\beta(x_i, x_f)$, and the right columns show the null distribution of S_β given by our permutation framework PASTEL.